

The Effect Components and Mechanisms of Action of Cimicifugae Rhizoma in the Treatment of Acute Pneumonia

Jing Zhu¹, Yiming Huang^{1,2}, Chao Ye³, Xiaoxia Deng^{1,2}, Yuxuan Zou^{1,2}, En Yuan², Qi Chen²

¹Research Center for Chinese Medicine Resources and Ethnic Minority Medicine, Jiangxi University of Chinese Medicine, Nanchang, People's Republic of China; ²School of Pharmacy, Jiangxi University of Chinese Medicine, Nanchang, People's Republic of China; ³The Affiliated Hospital of Jiangxi University of Chinese Medicine, Nanchang, People's Republic of China

Correspondence: Jing Zhu, Research Center for Chinese Medicine Resources and Ethnic Minority Medicine, Jiangxi University of Chinese Medicine, Nanchang, People's Republic of China, Tel +86-13755654318, Email 277836041@qq.com

Objective: The main objective of this study was to elucidate the effector material basis of Cimicifugae Rhizoma (CR) for the treatment of acute pneumonia (AP) and to explore the potential mechanisms underlying the anti-AP effects of these active components in a lipopolysaccharide (LPS)-induced inflammation model of lung epithelial cells.

Methods: Chemical components were identified using ultra-performance liquid chromatography-quadrupole-time-of-flight tandem mass spectrometry (UPLC-TOF-MS), and a CR component library was subsequently established based on a combination of databases and available literature. Bioinformatics techniques were used to construct “component-target” and “protein-protein interaction (PPI)” networks, and the potential active components and core targets screened according to degree value, followed by molecular docking and in vitro experiments for verification. Inflammation was induced in normal human lung epithelial cells using lipopolysaccharide (LPS) to mimic the occurrence of AP.

Results: In total, 122 CR components were identified. The therapeutic effects of potential active components against AP were associated with 147 targets involving 165 signaling pathways. Molecular docking experiments revealed the strong affinity of N-cis-feruloyltyramine, ferulic acid, cimifugin, and isoferulic acid for core AP-associated targets. In vitro cellular experiments showed that the above compounds and CR alcoholic extracts inhibited the expression of inflammatory factors in the following order: isoferulic acid > cimifugin > CR alcoholic extract > N-cis-feruloyltyramine > ferulic acid.

Conclusion: N-cis-feruloyltyramine, ferulic acid, cimifugin, and isoferulic acid were the effector components of CR with activity against AP. These compounds potentially co-regulate the IL-6/JAK/STAT3 and TLR4/IL-1 β -IRAK pathways through the inhibition of cytokines such as IL-6, TNF- α , and IL-1 β , and downregulation of P-STAT3, TLR4, PI3CA, and NF- κ B involved in TLR4/IL-1 β -IRAK/NF- κ B and PI3K-Akt signaling pathways to exert therapeutic effects on AP.

Keywords: acute pneumonia, molecule docking, lung epithelial cells, LPS, signaling pathway

Introduction

Acute pneumonia (AP) is a clinical condition caused by different pathogens following inhalation into the lungs, resulting in a serious decline in lung function and gradual development of acute respiratory distress syndrome (ARDS).¹ In situations where timely intervention is not provided, the condition can cause serious harm to patient health. Therefore, the suppression of lung inflammation may serve as a key strategy to alleviate AP. Antibiotics are generally used in the clinical treatment of AP; however, overuse can cause serious drug resistance. Bacterial drug resistance is currently a major public health problem worldwide and is characterized by a more rapid rate of development than antibacterial treatments.^{2,3} On the other hand, traditional Chinese medicine can delay the emergence of antibacterial drug resistance and help improve the immunity of patients, thus presenting a promising approach for the treatment of infectious diseases.

Chinese medicine, which has been used for hundreds of years, has accumulated extensive experience in treating a wide range of disorders. *Cimicifugae Rhizoma* (CR), a medicinal herb used in traditional Chinese medicine, effectively clears heat and removes toxins. Recent clinical studies have demonstrated that CR is a highly effective basic drug for treating patients with novel coronavirus-induced pneumonia.⁴ *Cimicifugae Rhizoma* (CR), a widely utilized medicinal material in traditional Chinese medicine, is renowned for its excellent heat-clearing and detoxifying properties.⁵ CR is derived from the dried rhizomes of plants *Cimicifuga heracleifolia* Kom., *Cimicifuga dahurica* (Turcz.) Maxim., or *Cimicifuga foetida* L., belonging to the Ranunculaceae family, and is highly valued for its distinctive medicinal qualities. CR contains triterpenes and their glycosides, phenolic acids, chromones, alkaloids, amides, sterols, sugars, volatile oils and other compounds, with anti-tumor, anti-inflammatory, anti-viral, anti-osteoporosis, hypoglycemic and lipid regulation, antioxidant, regulating the gastrointestinal and other aspects of pharmacological activity. In addition, CR has been successfully used to treat wind-heat headaches and sore throats. A substantial body of evidence from scientific studies has shown that drugs possessing heat-clearing and detoxifying properties exhibit significant anti-inflammatory effects. In traditional Chinese medicine (TCM), the primary site of action for the heat-clearing and detoxifying effects of *Cimicifugae Rhizoma*(CR) is believed to be the lungs. Consequently, this study selected pneumonia as the disease model to investigate the anti-inflammatory effects of CR, and to initially identify its anti-inflammatory effector substances and the mechanism of action.

In this study, we employed UPLC-MS technology to identify the chemical components in CR. These were then combined with the preliminary GC-MS results of the group, as well as the components in the TCM database and the literature, to establish a network pharmacological chemical component library. Bioinformatics methods were then used to predict the potential anti-AP active components. Finally, *in vitro* cellular experiments were carried out. The objective of this study is to verify the efficacy of CR in treating AP and to explore its mechanism of action. This will provide a foundation for subsequent *in vivo* studies and a scientific basis for the clinical application of Chinese medicine in the treatment of pneumonia-related diseases.

Materials and Methods

Analysis and Characterization of the Chemical Composition of CR

Ultra-performance liquid chromatography-quadrupole-time of flight tandem mass spectrometry (UPLC-Q-TOF-MS) in positive and negative ion modes was used to analyze the chemical composition of CR. Relative molecular mass, mass spectrometry cleavage patterns, and literature information were used to identify active constituent compounds.

Preparation of Test Solution

CR powder (0.5 g passed through a No.3 sieve) was weighed precisely and placed in a stoppered conical flask, followed by the addition of 10 mL 80% methanol aqueous solution. The mixture was weighed, subjected to ultrasonic extraction at 50°C for 40 min, cooled with 80% methanol to make up the weight. After filtration, 1 mL of the filtrate was centrifuged at 13000 rpm for 10 min and the supernatant fraction was isolated.

Chromatographic Conditions

An ACQUITY UPLC BEH C₁₈ column (2.1 × 100 mm, 1.7 μm) was employed with a mobile phase of 0.1% formic acid aqueous solution (A)–acetonitrile (B) gradient elution as follows: 0–1 min, 5% B; 1–20 min, 5–25% B; 20–35 min, 25–37% B; 35–38 min, 37% B; 38–40 min, 37–38% B; 40 to 48 min, 38–45% B; 48 to 68 min, 45–95% B; 68 to 70 min, 95% B; 70 to 70.1 min, 95–5% B; 70.1 to 75 min, 5% B. The column temperature was set at 40 °C, injection volume was 1 μL, and flow rate was 0.25 mL min⁻¹.

Mass Spectrometry Conditions

The apparatus included an electrospray ionization source (ESI) with positive and negative ion spray voltages (ISVF) of 5.5 kV and -4.5 kV, respectively. The experimental conditions were as follows: de-clustering voltage (DP), ±100 V; collision energy (CE), ±38 V; mass scanning range, *m/z* 100–1500; ionization source temperature (TEM), 500 °C; collision energy superposition (CES), 15 V; air curtain gas pressure (CUR), 40 psi; data acquisition time, 75 min; nebulizing gas pressure (GS1) 50 psi; auxiliary gas pressure (GS2), 50 psi.

Network Pharmacology and Molecular Docking Validation

Screening of the Potential Active Components of CR

The chemical constituents of CR were analyzed, and candidate compounds were identified by evaluating the prequel GC-MS⁵ in the early stage of the study and UPLC-MS in the present study. In view of the fact that the identified components do not represent the full range of active components in CR, we have also included those with biological activity that were not identified in our analysis but are reported in other literature. The constituents were searched in TCM databases such as SymMap, TCMID, TCMSP, and TCM-ID. The SwissADME (<http://www.swissadme.ch/>) and TCMSP (<http://lsp.nwu.edu.cn/tcmsp.Php>) database^{6,7} were imported and used to screen for potential active components of CR, with the Lipinski's Rule of Five,⁸ or a threshold set at oral utilization (OB) $\geq 30\%$ and drug-like properties (DL) ≥ 0.18 .⁹

Acquisition of CR Active Component Targets

The identified primary bioactive chemical components were uploaded in a molecular format to the SwissTarget Prediction database (<http://www.swisstargetprediction.ch/>). Specific parameters were set, such as species, Homosapiens, and the remaining parameters were set by default for SwissTarget prediction, filtered, and de-weighted with possibility >0 to obtain the targets of the CR components. The resulting targets were standardized to target genes using the UniProt database (<https://www.uniprot.org>) to obtain the official gene names, and subsequently merged and de-weighted to acquire the target information.

Acquisition of AP Corresponding Targets

The GeneCards (<https://www.genecards.org/>), DisGeNET (<https://www.disgenet.org/>), and OMIM databases (<http://www.omim.org/>) were utilized to screen AP targets based on the keyword “acutepneumonia”. The targets related to AP were downloaded, merged, and de-emphasized. The acquired AP and active component targets were re-screened to establish specific interacting molecules between CR and AP.^{10,11}

Construction and Analysis of Component and Target Networks

The CR components, together with the screened anti-pneumonia targets, were imported into Cytoscape 3.10.0 software to construct an “active component-target” network, whereby “node” represents the active component and target and “edge” represents the interaction between two nodes.

Protein Interaction (PPI) Network Construction and Analysis

The targets of the active component-AP interactions were imported into the Jvenn website (<http://www.bioinformatics.com.cn/static/others/jvenn/example.html>). The number of intersecting genes was illustrated using a Wayne diagram. Intersecting genes were imported into the STRING database (<https://string-db.org/cgi/input.pl>), the Homosapiens screening condition was set to hide the free targets, and the protein interaction score was set to 0.7. The data were exported in “TSV” format and uploaded to Cytoscape 3.10.0 software. A topology analysis was conducted to construct the PPI network.^{12,13}

GO Function and KEGG Pathway Enrichment Analyses of CR for Potential Active Components Against AP

The core targets of the potential active components of CR that exert therapeutic effects against AP were imported into the DAVID 6.8 data platform (<https://David.Nciferf.gov/>). The selected species was “Homosapiens”. GO function and KEGG pathway enrichment analyses were performed to obtain information on the associated biological processes and pathways, and the predicted pathways with activities against AP further visualized using the microbiotics platform (<https://www.bioinformatics.com.cn>).^{15–17} The significance level was set at $P < 0.05$.

Molecular Docking Validation

Using AutoDock software, the core target protein was dehydrogenated, hydrogenated, selected as the receptor, and exported in “PDBQT” format, while the potential core component was hydrogenated, selected as ligand, and exported in the same format. The docking box was set and saved, and Vina ran to sequentially dock the active component with the protein to obtain binding energy, followed by heat map analysis. The PyMOL software was used to view the 3D spatial conformation of the molecular docking complex.^{17,18}

Cellular Experimental Validation of the Efficacy of CR

Experimental Materials

BEAS-2B cells (Cat. No. CRL9609) were obtained from the American Type Culture Collection (ATCC) located in Manassas, VA, USA. ZQXZbio (Shanghai, China) provided Dulbecco's modified Eagle's medium (DMEM), fetal bovine serum, phosphate-buffered saline (PBS), trypsin, and dual-antibiotics. Meilunbio (Liaoning, China) provided the CCK-8 cell viability and cytotoxicity test kit. LPS was obtained from Sigma–Aldrich (St. Louis, MO, USA). IL-6, IL-1 β , and TNF- α kits were purchased from Quanzhou Ruixin Biotechnology Co., Ltd. (Quanzhou, China) and qPCR kits were purchased from Beijing ComWin Biotech Co., Ltd. (Beijing, China). Primers were synthesized by Shanghai Sangong Bioengineering Co. Ltd. The experiments also used The BCA protein quantification kit (Labgic Technology Co., Ltd., Hefei, China), QuickBlock Western Closure Solution, QuickBlock Western Primary Antibody Dilution, and QuickBlock Western Secondary Antibody Dilution were purchased from Beyotime Biotechnology (Shanghai, China). Toll-like receptor 4 (TLR4) (Cat. 66350-1-Ig), Signal transducer and activator of transcription 3 (STAT3) (Cat. 10253-2-AP), glyceraldehyde 3-phosphate dehydrogenase (GAPDH) (Cat. 60004-1-Ig), Phosphatidylinositol-4,5-Bisphosphate 3-Kinase Catalytic Subunit Alpha (PIK3CA) (Cat. AF4669), Heat Shock Protein 90 Alpha Family Class A Member 1 (HSP90AA1) (Cat. BF0084) and phosphorylation- Signal transducer and activator of transcription 3 (P-STAT3) (Cat. AF3293) were obtained from Beyotime Biotechnology (Shanghai, China).

Preparation of Complete Culture Medium

FBS was incubated at room temperature and mixed with DMEM-H basal medium and penicillin/streptomycin double antibody at a 10%: 90%: 1% proportion to generate complete culture medium, which was stored at 4 °C until experimental use.

Preparation of Cell Cryopreservation Solution

BEAS-2B cells were prepared by mixing FBS and DMSO at a 9:1 ratio in sterile centrifuge tubes.

Preparation of LPS Solution

LPS powder (50 μ g) was dissolved in 1 mL PBS to produce a 50 μ g/mL stock solution. The solution was filtered, decontaminated using a 0.22 μ m filter, and dispensed as required.

Cell Culture

BEAS-2B cells were cultured in medium containing 10% fetal bovine serum. The cells were maintained in an incubator under optimal growth conditions (37°C, 5% CO₂, and a humidified atmosphere). The frequency of fluid change was dictated by the growth parameters of BEAS-2B cells, which were generally sufficient for two days. The medium was replaced with complete medium every two days to continue the culture or transferred to cell plates in preparation for experiments, such as drug administration.

CCK-8 Cell Viability Assay

BEAS-2B cells were harvested during the logarithmic growth phase and seeded in 96-well plates at a density of 1×10^6 cells/well. After stimulation of cells with LPS (25, 50, 75, 100, and 125 μ g/mL), 10 μ L of CCK-8 was added to each well, and the plates were incubated for an additional 1.5 h. Absorbance at 450 nm was measured using a SpectraMax™ M2 reader (using 600 nm as the reference wavelength). Culture medium without cells was used as the blank sample. Cell survival was calculated as the absorbance of treated cells/absorbance of control cells \times 100.

ELISA of the Effects of Potential Active Components on LPS-Induced Cytokine Expression

EAS-2B cells were inoculated in six-well plates, cell concentrations were adjusted to 2×10^5 cells/well, and 2 mL of basal medium was added to the culture. Next, the cells were stimulated to produce an inflammatory response with 50 μ g/mL LPS. Cells in each group were randomly divided into control, model, N-cis-feruloyltyramine (6.25 μ g/mL), ferulic acid (6.25 μ g/mL), cimifugin (6.25 μ g/mL), isoferulic acid (6.25 μ g/mL), positive drug (50 μ g/mL), CR alcohol extract (6.25 μ g/mL), and normal groups (cells are cultured normally without molding). Cells in each group were cultured in a constant-temperature incubator at 37°C with 5% CO₂ for 24 h. The supernatant fractions of the cells in each group were

collected in sterile tubes and centrifuge at 4000rpm for 20 min to remove cell pellets and polymers. The IL-6, TNF- α , and PIK3CA protein levels were measured according to the instructions of the ELISA instructions.

RT-qPCR Analysis of the Effects of Treatments on LPS-Induced Cytokine mRNA Expression

Total RNA was extracted using TRIzol® reagent (TransGen Biotech, Beijing, China) and reverse-transcribed using EasyScript® reverse transcriptase, according to the manufacturer's instructions. The primer information is presented in Table 1.

Western Blot Analysis of the Effects of Potential Active Components on Protein Expression in the Inflammation Model

Total protein was extracted using radioimmunoprecipitation assay (RIPA) lysis buffer, and protein concentrations were determined using a BCA Protein Quantification Kit (Biosharp, Anhui, China). Cell lysates containing equal amounts of proteins were separated by electrophoresis using a FuturePAGE™ protein prep gel, followed by transfer to polyvinylidene fluoride (PVDF) membranes. After blocking with rapid closure solution for 5–15 min at room temperature, the membrane was incubated with a 1:10,000 dilution of the primary antibody at 4°C overnight and a 1:10,000 dilution of the secondary antibody at 37°C for 1 h (TLR4, PIK3CA, HSP90AA1, STAT3, and p-STAT3). Equal amounts of ECL luminescent solutions A and B were thoroughly mixed for 5 min and placed in front of the membrane in a dark room to avoid light. The color development solution was carefully aspirated with paper, the top was covered with flat transparent paper, and placed in a dark box, followed by scanning and analysis.

Statistical Analyses

Measurement data are expressed as the mean \pm standard deviation. Prism 10.1.2 (GraphPad, San Diego, CA, United States) was used for one-way ANOVA to determine the significance of results. The following nomenclature was used to indicate significance levels in figures: * $P < 0.05$, ** $P < 0.01$, *** $P < 0.001$, **** $P < 0.0001$. All experiments were repeated at least three times.

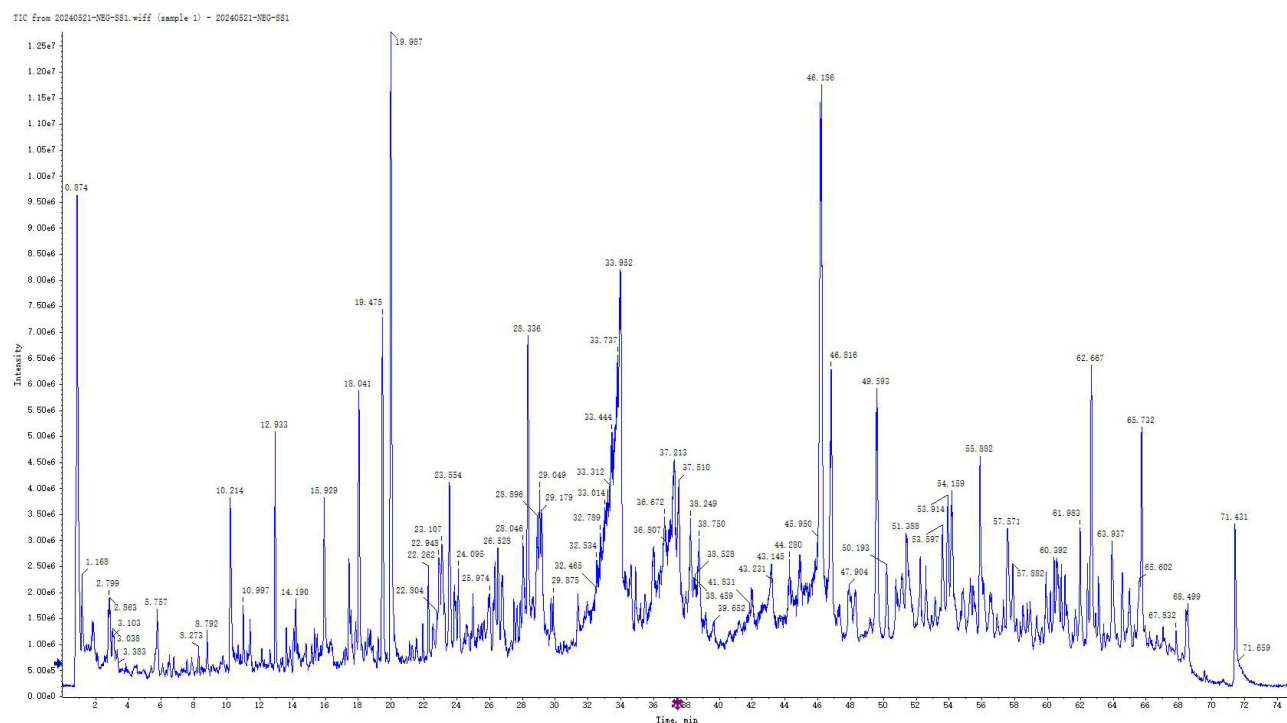
Experimental Results

Identification of CR Components via UPLC-QTOF-MS/MS

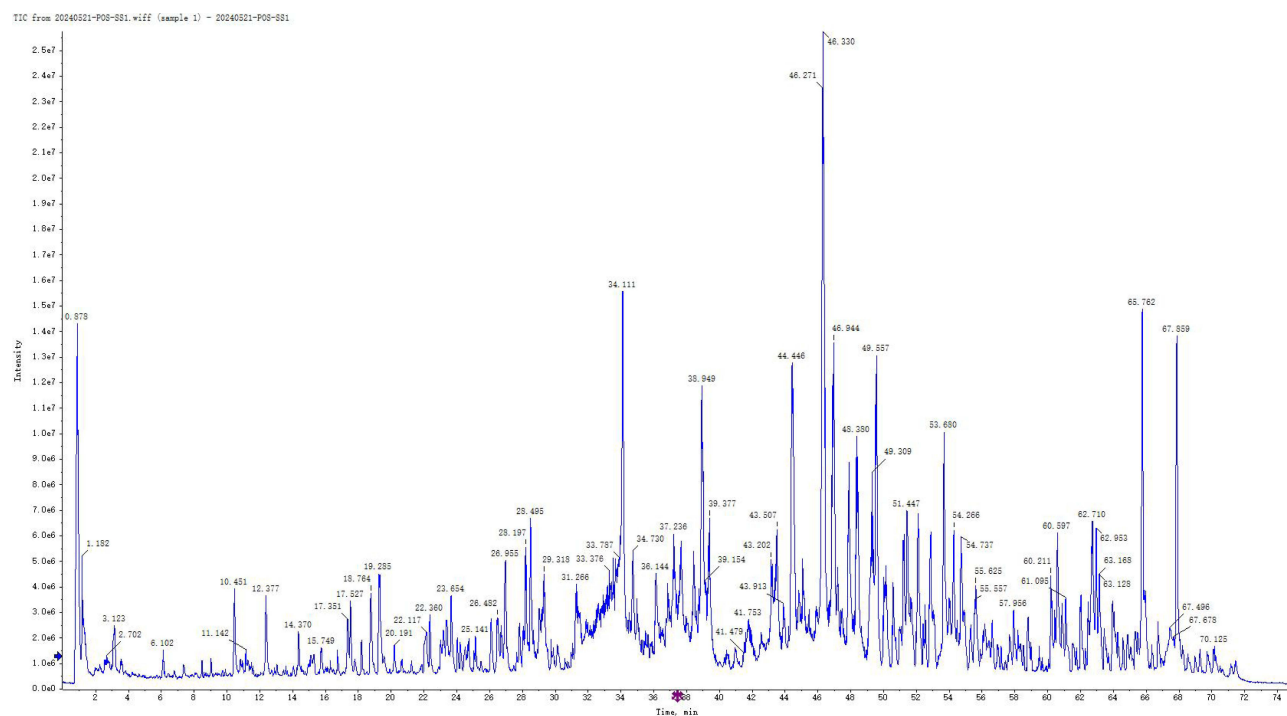
Samples were injected according to the conditions specified in Sections 2.1, and the total ion flow diagrams of the positive and negative ions of the raw products of CR were obtained (Figure 1). After reviewing the relevant literature, a database of CR chemical components was established using the TCM databases SymMap, TCMID, TCMSP, and TCM-ID. Phenolic acids, triterpenoids, chromones, and alkaloids with a mass deviation of less than 5×10^{-6} were initially screened using the PeakView software, leading to the identification of 122 compounds (Table 2).

Table 1 Primer Information

Gene Name	Primer Name	Primer Sequence (5'-3')	Product Length (bp)
GADPH	Human-GAPDH-F	TGACTTCAACAGCGACACCCA	121
	Human-GAPDH-R	CACCCTGTTGCTGTAGCCAAA	
TLR4	Hsa-TLR4 F	GTCGGTCCTCAGTGTGCTTGTAG	216
	Hsa-TLR4 R	TGAAGGCAGAGCTGAAATGGAGG	
PIK3CA	Hsa-PIK3CA F	ACGCATTTCCACAGCTACACCAT	273
	Hsa-PIK3CA R	GCAGCACGAGGAAGATCAGGAAT	
HSP90AA1	Hsa-HSP90AA1 F	TGAAACTGCGCTCCTGTCTTCTG	190
	Hsa-HSP90AA1 R	TTCTTCCATGCGTGATGTGTCGT	



A. CR raw product in the negative ion mode



B. CR raw product in the positive ion mode

Figure 1 Representative base peak chromatograms of CR in the negative (A) and positive ionization modes (B), respectively.

Table 2 Characterization of the Chemical Constituents of CR via Ultra-Performance Liquid Chromatography Quadrupole Time-of-Flight Tandem Mass Spectrometry

No.	Formula	Components	ESI	m/z Theoretical Value	m/z Actual Value	Error	Fragments	tR/ min
1	C ₁₂ H ₂₂ O ₁₁	Sucrose	[M-H] ⁻	341.10894	341.10926	1	179.0350[C ₉ H ₇ O ₄] ⁻ , 119.0520[C ₈ H ₇ O] ⁻ , 95.0139[C ₅ H ₃ O ₂] ⁻ , 71.0139 [C ₃ H ₃ O ₂] ⁻	0.86
2	C ₁₇ H ₂₆ O ₁₁	Shanzhiside methyl ester	[M-H] ⁻	405.14024	405.13985	-1	359.0984[C ₁₅ H ₁₉ O ₁₀] ⁻ , 197.0819[C ₁₀ H ₁₃ O ₄] ⁻ , 179.0561[C ₆ H ₁₁ O ₆] ⁻ , 161.0455 [C ₆ H ₉ O ₅] ⁻ , 101.0244[C ₄ H ₅ O ₃] ⁻	1.72
3	C ₁₁ H ₁₂ O ₇	Piscidic acid	[M-H] ⁻	255.05103	255.05185	3.2	255.0510[C ₁₁ H ₁₁ O ₇] ⁻ , 193.0506[C ₁₀ H ₉ O ₄] ⁻ , 165.0557[C ₉ H ₉ O ₃] ⁻ , 149.0092 [C ₄ H ₅ O ₆] ⁻ , 133.0295[C ₈ H ₅ O ₂] ⁻ , 93.0346[C ₆ H ₅ O] ⁻ , 72.9931[C ₂ H ₃ O ₃] ⁻	2.84
4	C ₁₄ H ₂₀ O ₈	Cimidahurinine	[M-H] ⁻	315.10854	315.10879	0.8	153.0557[C ₈ H ₉ O ₃] ⁻ , 123.0452[C ₇ H ₇ O ₂] ⁻	3.07
5	C ₁₄ H ₂₀ O ₈	Grevilloside G	[M-H] ⁻	315.10854	315.10879	0.8	153.0557[C ₈ H ₉ O ₃] ⁻ , 123.0452[C ₇ H ₇ O ₂] ⁻	3.30
6	C ₁₄ H ₁₈ O ₈	alopecuquinone	[M-H] ⁻	313.09289	313.09278	-0.4	277.0718[C ₁₄ H ₁₃ O ₆] ⁻ , 178.8840[C ₇ H ₁₅ O ₅] ⁻ , 107.0139[C ₆ H ₃ O ₂] ⁻ , 71.0139 [C ₃ H ₃ O ₂] ⁻ , 59.0139[C ₂ H ₃ O ₂] ⁻	3.38
7	C ₁₉ H ₂₈ O ₁₂	8-O-acetylshanzhisidemethylester	[M-H] ⁻	447.1508	447.14975	-2.4	401.1089[C ₁₇ H ₂₁ O ₁₁] ⁻ , 269.1031[C ₁₃ H ₁₇ O ₆] ⁻ , 161.0455[C ₆ H ₉ O ₅] ⁻	8.48
8	C ₂₁ H ₂₀ O ₁₂	Hyperoside	[M-H] ⁻	463.0882	463.08701	-2.6	179.0561[C ₆ H ₁₁ O ₆] ⁻ , 163.0424[C ₆ H ₁₁ O ₅] ⁻ , 137.0244[C ₇ H ₅ O ₃] ⁻ , 109.0295 [C ₆ H ₅ O ₂] ⁻	10.42
9	C ₂₄ H ₂₉ NO ₁₀	Cimicifugamide A	[M-H] ⁻	490.17187	490.17077	-2.3	328.1190[C ₁₈ H ₁₈ NO ₅] ⁻ , 178.0510[C ₉ H ₈ NO ₃] ⁻	11.41
10	C ₂₇ H ₃₀ O ₁₆	Shomaside A	[M-H] ⁻	609.14611	609.14471	-2.3	609.1461[C ₂₇ H ₂₉ O ₁₆] ⁻ , 253.0354[C ₁₁ H ₉ O ₇] ⁻ , 235.0248[C ₁₁ H ₇ O ₆] ⁻ , 191.0350 [C ₁₀ H ₇ O ₄] ⁻ , 189.0041[C ₆ H ₅ O ₇] ⁻ , 181.0506[C ₉ H ₉ O ₄] ⁻	11.42
11	C ₂₅ H ₃₁ NO ₁₀	Cimidahurine	[M-H] ⁻	504.18752	504.18662	-1.8	342.1347[C ₁₉ H ₂₀ NO ₅] ⁻ , 178.0510[C ₉ H ₈ NO ₃] ⁻ , 148.0768[C ₉ H ₁₀ NO] ⁻	12.64
12	C ₂₇ H ₃₀ O ₁₅	Shomaside C	[M-H] ⁻	593.15119	593.14972	-2.5	593.1512[C ₂₇ H ₂₉ O ₁₅] ⁻ , 237.0405[C ₁₁ H ₉ O ₆] ⁻ , 193.0506[C ₁₀ H ₉ O ₄] ⁻ , 165.0557 [C ₉ H ₉ O ₃] ⁻ , 149.0455[C ₅ H ₉ O ₅] ⁻	12.94
13	C ₁₈ H ₁₆ O ₁₀	Cimicifugic acid H	[M-H] ⁻	391.06707	391.06672	-0.9	391.0671[C ₁₈ H ₁₅ O ₁₀] ⁻ , 271.0459[C ₁₁ H ₁₁ O ₈] ⁻ , 253.0354[C ₁₁ H ₉ O ₇] ⁻ , 191.0197 [C ₆ H ₇ O ₇] ⁻ , 181.0506[C ₉ H ₉ O ₄] ⁻	13.31
14	C ₂₄ H ₂₉ NO ₉	Demethoxycimicifugamide	[M-H] ⁻	474.17696	474.17588	-2.3	312.1241[C ₁₈ H ₁₈ NO ₄] ⁻ , 297.0980[C ₁₄ H ₁₇ O ₇] ⁻ , 148.0768[C ₉ H ₁₀ NO] ⁻	13.39
15	C ₁₂ H ₈ O ₅	Norkhellol	[M-H] ⁻	231.0299	231.03048	2.5	203.0350[C ₁₁ H ₇ O ₄] ⁻ , 187.0037[C ₁₀ H ₃ O ₄] ⁻ , 185.0244[C ₁₁ H ₅ O ₃] ⁻ , 161.0244 [C ₉ H ₅ O ₃] ⁻ , 149.0244[C ₈ H ₅ O ₃] ⁻	13.64

(Continued)

Table 2 (Continued).

No.	Formula	Components	ESI	m/z Theoretical Value	m/z Actual Value	Error	Fragments	tR/ min
16	C ₂₇ H ₃₀ O ₁₆	Kaempferol 3,7-diglucoside	[M-H] ⁻	609.14611	609.14427	-3	609.1461[C ₂₇ H ₂₉ O ₁₆] ⁻ , 253.0506[C ₁₅ H ₉ O ₄] ⁻ , 191.0561[C ₇ H ₁₁ O ₆] ⁻ , 189.0405[C ₇ H ₉ O ₆] ⁻	13.75
17	C ₂₀ H ₁₈ O ₁₁	Fukinolic acid	[M-H] ⁻	433.07764	433.07685	-1.8	271.0459[C ₁₁ H ₁₁ O ₈] ⁻ , 253.0354[C ₁₁ H ₉ O ₇] ⁻ , 191.0350[CH ₇ O ₄] ⁻ , 181.0506[C ₉ H ₉ O ₄] ⁻ , 179.0350[C ₉ H ₇ O ₄] ⁻ , 135.0452[C ₈ H ₇ O ₂] ⁻ , 123.0452[C ₇ H ₇ O ₂] ⁻	14.06
18	C ₂₅ H ₃₁ NO ₁₀	Isocimicifugamide	[M-H] ⁻	504.18752	504.18611	-2.8	342.1347[C ₁₉ H ₂₀ NO ₅] ⁻ , 178.0510[C ₉ H ₈ NO ₃] ⁻ , 148.0768[C ₉ H ₁₀ NO] ⁻	14.10
19	C ₂₅ H ₃₁ NO ₁₀	Cimicifugamide	[M-H] ⁻	504.18752	504.18611	-2.8	342.1347[C ₁₉ H ₂₀ N ₅ O] ⁻ , 178.0510[C ₉ H ₈ NO ₃] ⁻ , 148.0768[C ₉ H ₁₀ NO] ⁻	14.19
20	C ₂₃ H ₂₆ O ₁₄	Norkhelloside	[M-H] ⁻	525.12498	525.12315	-3.5	525.1250[C ₂₃ H ₂₅ O ₁₄] ⁻ , 273.0405[C ₁₄ H ₉ O ₆] ⁻ , 243.0299[C ₁₃ H ₇ O ₅] ⁻ , 229.0142[C ₁₂ H ₅ O ₅] ⁻	15.47
21	C ₂₇ H ₃₀ O ₁₆	Sophoraflavonolside	[M-H] ⁻	609.14611	609.14388	-3.7	609.1461[C ₂₇ H ₂₉ O ₁₆] ⁻ , 415.0671[C ₂₀ H ₁₅ O ₁₀] ⁻ , 253.0506[C ₁₅ H ₉ O ₄] ⁻ , 191.0561[C ₇ H ₁₁ O ₆] ⁻	15.55
22	C ₂₀ H ₁₈ O ₁₀	Cimicifugic acid D	[M-H] ⁻	417.08272	417.08204	-1.6	255.0510[C ₁₁ H ₁₁ O ₇] ⁻ , 193.0506[C ₁₀ H ₉ O ₄] ⁻ , 179.0350[C ₉ H ₇ O ₄] ⁻ , 165.0557[C ₉ H ₉ O ₃] ⁻ , 149.0092[C ₄ H ₅ O ₆] ⁻ , 135.0452[C ₈ H ₇ O ₂] ⁻	15.93
23	C ₂₀ H ₁₈ O ₁₀	Cimicifugic acid C	[M-H] ⁻	417.08272	417.08204	-1.6	255.0510[C ₁₁ H ₁₁ O ₇] ⁻ , 179.0350[C ₉ H ₇ O ₄] ⁻ , 149.0244[C ₈ H ₅ O ₃] ⁻	16.41
24	C ₂₂ H ₂₂ O ₁₂	Cimicifugic acid I	[M-H] ⁻	477.10385	477.10265	-2.5	253.0354[C ₁₁ H ₉ O ₇] ⁻ , 235.0612[C ₁₂ H ₁₁ O ₅] ⁻ , 165.0557[C ₉ H ₉ O ₃] ⁻ , 163.0401[C ₉ H ₇ O ₃] ⁻ , 151.0401[C ₈ H ₇ O ₃] ⁻ , 123.0452[C ₇ H ₇ O ₂] ⁻ , 109.0295[C ₆ H ₅ O ₂] ⁻	17.23
25	C ₂₁ H ₂₀ O ₁₁	Cimicifugic acid A	[M-H] ⁻	447.09329	447.0926	-1.5	253.0354[C ₁₁ H ₉ O ₇] ⁻ , 235.0248[C ₁₁ H ₇ O ₆] ⁻ , 191.0350[C ₁₀ H ₇ O ₄] ⁻ , 173.0244[C ₁₀ H ₅ O ₃] ⁻ , 163.0401[C ₉ H ₇ O ₃] ⁻ , 151.0401[C ₈ H ₇ O ₃] ⁻	17.44
26	C ₂₁ H ₂₀ O ₁₁	Cimicifugic acid B	[M-H] ⁻	447.09329	447.0926	-1.5	235.0354[C ₁₁ H ₉ O ₇] ⁻ , 189.0041[C ₆ H ₅ O ₇] ⁻ , 181.0506[C ₉ H ₉ O ₄] ⁻ , 173.0244[C ₁₀ H ₅ O ₃] ⁻ , 163.0401[C ₉ H ₇ O ₃] ⁻ , 151.0401[C ₈ H ₇ O ₃] ⁻ , 123.0452[C ₇ H ₇ O ₂] ⁻ , 109.0295[C ₆ H ₅ O ₂] ⁻	18.04
27	C ₂₁ H ₂₀ O ₁₁	24-O-acetylhydroshengmanol 3-O-β-D-xylopyranoside	[M-H] ⁻	447.09329	447.0926	-1.5	191.0925[C ₈ H ₁₅ O ₅] ⁻ , 173.0819[C ₈ H ₁₃ O ₄] ⁻ , 163.0612[C ₆ H ₁₁ O ₅] ⁻ , 145.0870[C ₇ H ₁₃ O ₃] ⁻	18.38
28	C ₁₈ H ₁₉ NO ₄	N-cis-feruloyltyramine	[M-H] ⁻	312.12413	312.12458	1.4	312.1241[C ₁₈ H ₁₈ NO ₄] ⁻ , 190.0510[C ₁₀ H ₈ NO ₃] ⁻ , 178.0510[C ₉ H ₈ NO ₃] ⁻ , 148.0768[C ₉ H ₁₀ NO] ⁻ , 147.0452[C ₉ H ₇ O ₂] ⁻ , 135.0452[C ₈ H ₇ O ₂] ⁻ , 134.0611[C ₈ H ₈ NO] ⁻	18.59
29	C ₂₂ H ₂₂ O ₁₁	Cimicifugic acid J	[M-H] ⁻	461.10894	461.10772	-2.6	223.0612[C ₁₁ H ₁₁ O ₅] ⁻ , 193.0506[C ₁₀ H ₉ O ₄] ⁻ , 165.0557[C ₉ H ₉ O ₃] ⁻ , 149.0608[C ₉ H ₉ O ₂] ⁻ , 147.0452[C ₉ H ₇ O ₂] ⁻ , 107.0502[C ₇ H ₇ O] ⁻	19.20

30	C ₂₁ H ₂₀ O ₁₀	Cimicifugic acid F	[M-H] ⁻	431.09837	431.09788	-1.1	193.0506[C ₁₀ H ₉ O ₄] ⁻ , 165.0557[C ₉ H ₉ O ₃] ⁻ , 149.0608[C ₉ H ₉ O ₂] ⁻	19.47
31	C ₂₁ H ₂₀ O ₁₀	Cimicifugic acid E	[M-H] ⁻	431.09837	431.09788	-1.1	193.0506[C ₁₀ H ₉ O ₄] ⁻ , 165.0557[C ₉ H ₉ O ₃] ⁻ , 149.0608[C ₉ H ₉ O ₂] ⁻	19.99
32	C ₂₃ H ₂₈ O ₁₁	Paeoniflorin	[M-H] ⁻	479.15589	479.15454	-2.8	479.1559[C ₂₃ H ₂₇ O ₁₁] ⁻ , 241.0718[CC ₁₁ H ₁₃ O ₆] ⁻ , 197.0819 [C ₁₀ H ₁₃ O ₄] ⁻ , 193.0506[C ₁₀ H ₉ O ₄] ⁻ , 181.0506[C ₉ H ₉ O ₄] ⁻ , 165.0557 [C ₉ H ₉ O ₃] ⁻ , 149.0455[C ₅ H ₉ O ₅] ⁻ , 59.0139[C ₂ H ₃ O ₂] ⁻	21.28
33	C ₁₈ H ₁₆ O ₇	cimiciphenone	[M-H] ⁻	343.08233	343.08256	0.7	343.0823[C ₁₈ H ₁₅ O ₇] ⁻ , 193.0506[C ₁₀ H ₉ O ₄] ⁻ , 149.0608[C ₉ H ₉ O ₂] ⁻ , 121.0295 [C ₇ H ₅ O ₂] ⁻	22.96
34	C ₄₁ H ₆₄ O ₁₅	Heracleifolinoside C	[M-H] ⁻	795.41725	795.41527	-2.5	795.4171[C ₄₁ H ₆₃ O ₁₅] ⁻ , 615.3539[C ₃₅ H ₅₁ O ₉] ⁻ , 501.322[C ₃₀ H ₄₅ O ₆] ⁻ , 369.2435 [C ₂₄ H ₃₃ O ₃] ⁻ , 179.0561[C ₆ H ₁₁ O ₆] ⁻	23.53
35	C ₂₅ H ₃₀ O ₁₁	Shomaside E	[M-H] ⁻	505.17154	505.16997	-3.1	505.1715[C ₂₅ H ₂₉ O ₁₁] ⁻ , 267.0874[C ₁₃ H ₁₅ O ₆] ⁻ , 255.0874 [C ₁₂ H ₁₅ O ₆] ⁻ , 193.0506[C ₁₀ H ₉ O ₄] ⁻ , 175.0401[C ₁₀ H ₇ O ₃] ⁻ , 165.0557 [C ₉ H ₉ O ₃] ⁻ , 149.0608[C ₉ H ₉ O ₂] ⁻ , 59.0139[C ₂ H ₃ O ₂] ⁻	24.16
36	C ₃₅ H ₅₄ O ₁₀	Cimicifugoside H-2	[M-H] ⁻	633.36442	633.36233	-3.3	633.3644[C ₃₅ H ₅₃ O ₁₀] ⁻ , 589.3382[C ₃₃ H ₄₉ O ₉] ⁻ , 575.3226 [C ₃₂ H ₄₇ O ₉] ⁻ , 369.2435[C ₂₄ H ₃₃ O ₃] ⁻	25.89
37	C ₁₁ H ₁₀ O ₅	4-O-acetyl caffeic acid	[M-H] ⁻	221.04555	221.04613	2.6	203.0350[C ₁₁ H ₇ O ₄] ⁻ , 149.0244[C ₈ H ₅ O ₃] ⁻	26.02
38	C ₃₅ H ₅₄ O ₁₀	Bugbanoside B	[M-H] ⁻	633.36442	633.36244	-3.1	501.3222[C ₃₀ H ₄₅ O ₆] ⁻ , 501.3222[C ₃₀ H ₄₅ O ₆] ⁻ , 369.2283[C ₂₀ H ₃₃ O ₆] ⁻	28.34
39	C ₃₇ H ₅₈ O ₁₂	Cimidahuside C	[M-H] ⁻	693.38555	693.38311	-3.5	693.3856[C ₃₇ H ₅₇ O ₁₂] ⁻ , 651.3750[C ₃₅ H ₅₅ O ₁₁] ⁻ , 633.3644[C ₃₅ H ₅₃ O ₁₀] ⁻	29.17
40	C ₃₇ H ₅₆ O ₁₁	Actein	[M-H] ⁻	675.37499	675.37301	-2.9	617.3331[C ₃₄ H ₄₉ O ₁₀] ⁻ , 615.3539[C ₃₅ H ₅₁ O ₉] ⁻ , 599.3226 [C ₃₄ H ₄₇ O ₉] ⁻ , 543.2963[C ₃₁ H ₄₃ O ₈] ⁻ , 539.3014[C ₃₂ H ₄₃ O ₇] ⁻ , 517.3171 [C ₃₀ H ₄₅ O ₇] ⁻ , 483.3116[C ₃₀ H ₄₃ O ₅] ⁻ , 131.0350[C ₅ H ₇ O ₄] ⁻	31.24
41	C ₃₇ H ₅₆ O ₁₁	Cimidahuside J	[M-H] ⁻	675.37499	675.37301	-2.9	617.3331[C ₃₄ H ₄₉ O ₁₀] ⁻ , 615.3539[C ₃₅ H ₅₁ O ₉] ⁻ , 599.3226 [C ₃₄ H ₄₇ O ₉] ⁻ , 543.2963[C ₃₁ H ₄₃ O ₈] ⁻ , 539.3014[C ₃₂ H ₄₃ O ₇] ⁻ , 517.3171 [C ₃₀ H ₄₅ O ₇] ⁻ , 501.3222[C ₃₀ H ₄₅ O ₆] ⁻ , 483.3116[C ₃₀ H ₄₃ O ₅] ⁻	31.38
42	C ₃₅ H ₅₂ O ₉	Cimidahuside F	[M-H] ⁻	615.35386	615.35171	-3.5	615.3539[C ₃₅ H ₅₁ O ₉] ⁻ , 557.1301[C ₂₇ H ₂₅ O ₁₃] ⁻ , 483.3116 [C ₃₀ H ₄₃ O ₅] ⁻ , 471.0780[C ₁₉ H ₁₉ O ₁₄] ⁻ , 331.1707[C ₁₉ H ₂₅ O ₅] ⁻	31.38
43	C ₃₇ H ₅₆ O ₁₁	Bugbanoside A	[M-H] ⁻	675.37499	675.37301	-2.9	617.3331[C ₃₄ H ₄₉ O ₁₀] ⁻ , 615.3539[C ₃₅ H ₅₁ O ₉] ⁻ , 599.3226 [C ₃₄ H ₄₇ O ₉] ⁻ , 543.2963[C ₃₁ H ₄₃ O ₈] ⁻ , 539.3014[C ₃₂ H ₄₃ O ₇] ⁻ , 131.0350 [C ₅ H ₇ O ₄] ⁻ , 73.0295[C ₃ H ₅ O ₂] ⁻ , 59.0139[C ₂ H ₃ O ₂] ⁻	31.39

(Continued)

Table 2 (Continued).

No.	Formula	Components	ESI	m/z Theoretical Value	m/z Actual Value	Error	Fragments	tR/ min
44	C ₃₇ H ₅₆ O ₁₁	CimiracemosideG	[M-H] ⁻	675.37499	675.37301	-2.9	617.3331[C ₃₄ H ₄₉ O ₁₀] ⁻ , 615.3539[C ₃₅ H ₅₁ O ₉] ⁻ , 599.3226 [C ₃₄ H ₄₇ O ₉] ⁻ , 543.2963[C ₃₁ H ₄₃ O ₈] ⁻ , 483.3116[C ₃₀ H ₄₃ O ₅] ⁻ , 131.0350 [C ₅ H ₇ O ₄] ⁻ , 73.0295[C ₃ H ₅ O ₂] ⁻	31.80
45	C ₁₅ H ₁₆ O ₅	Visamminol	[M-H] ⁻	275.0925	275.09266	0.6	275.0925[C ₁₅ H ₁₅ O ₅] ⁻ , 259.0612[C ₁₄ H ₁₁ O ₅] ⁻ , 243.0663[C ₁₄ H ₁₁ O ₄] ⁻ , 241.0870 [C ₁₅ H ₁₃ O ₃] ⁻ , 201.0193[C ₁₁ H ₅ O ₄] ⁻ , 173.0244[C ₁₀ H ₅ O ₃] ⁻	31.87
46	C ₃₀ H ₄₆ O ₆	12β-hydroxy-7(8)-ene-cimigenol	[M-H] ⁻	501.32216	501.32022	-3.9	501.3222[C ₃₀ H ₄₅ O ₆] ⁻ , 457.2959[C ₂₈ H ₄₁ O ₅] ⁻ , 443.2803[C ₂₇ H ₃₉ O ₅] ⁻ , 399.2177 [C ₂₄ H ₃₁ O ₅] ⁻ , 99.0815[C ₆ H ₁₁ O] ⁻ , 73.0659[C ₄ H ₉ O] ⁻	31.90
47	C ₃₇ H ₅₆ O ₁₁	Actaeaepoxide-3-O-β-D-xylopyranoside	[M-H] ⁻	675.37499	675.37301	-2.9	617.3331[C ₃₄ H ₄₉ O ₁₀] ⁻ , 615.3539[C ₃₅ H ₅₁ O ₉] ⁻ , 599.3226 [C ₃₄ H ₄₇ O ₉] ⁻ , 543.2963[C ₃₁ H ₄₃ O ₈] ⁻ , 539.3014[C ₃₂ H ₄₃ O ₇] ⁻ , 501.3222 [C ₃₀ H ₄₅ O ₆] ⁻ , 483.3116[C ₃₀ H ₄₃ O ₅] ⁻ , 131.0350[C ₅ H ₇ O ₄] ⁻	31.92
48	C ₃₇ H ₅₄ O ₁₁	Cimiracemoside P	[M-H] ⁻	673.35934	673.3585	-1.2	673.3593[C ₃₇ H ₅₃ O ₁₁] ⁻ , 637.3382[C ₃₇ H ₄₉ O ₉] ⁻	33.91
49	C ₃₇ H ₅₄ O ₁₁	Cimicifugoside	[M-H] ⁻	673.35934	673.3585	-1.2	673.3593[C ₃₇ H ₅₃ O ₁₁] ⁻ , 637.3382[C ₃₇ H ₄₉ O ₉] ⁻	33.91
50	C ₄₃ H ₆₈ O ₁₆	Heracleifolinoside F	[M-H] ⁻	839.44346	839.44153	-2.3	839.4435[C ₄₃ H ₆₇ O ₁₆] ⁻ , 779.4223[C ₄₁ H ₆₃ O ₁₄] ⁻	34.91
51	C ₃₀ H ₄₆ O ₆	7,8-Didehydrocimigenol	[M-H] ⁻	501.32216	501.32022	-3.9	501.3222[C ₃₀ H ₄₅ O ₆] ⁻ , 443.2803[C ₂₇ H ₃₉ O ₅] ⁻ , 425.2697[C ₂₇ H ₃₇ O ₄] ⁻ , 99.0815 [C ₆ H ₁₁ O] ⁻ , 73.0659[C ₄ H ₉ O] ⁻	35.47
52	C ₃₆ H ₅₈ O ₁₁	Cimifoetiside I	[M-H] ⁻	665.39064	665.38799	-4	665.3906[C ₃₆ H ₅₇ O ₁₁] ⁻ , 619.3488[C ₃₄ H ₅₁ O ₁₀] ⁻	38.24
53	C ₁₅ H ₁₆ O ₄	Peucenin	[M-H] ⁻	259.09758	259.09782	0.9	259.0976[C ₁₅ H ₁₅ O ₄] ⁻ , 243.0663[C ₁₄ H ₁₁ O ₄] ⁻ , 215.0714[C ₁₃ H ₁₁ O ₃] ⁻ , 203.0350 [C ₁₁ H ₇ O ₄] ⁻ , 175.0765[C ₁₁ H ₁₁ O ₂] ⁻	39.09
54	C ₃₆ H ₅₈ O ₁₀	Cimifoetiside II	[M-H] ⁻	649.39572	649.39468	-1.6	649.3957[C ₃₆ H ₅₇ O ₁₀] ⁻ , 487.3429[C ₃₀ H ₄₇ O ₅] ⁻	45.98
55	C ₃₇ H ₅₈ O ₁₁	12β-acetoxycimigenol-3-O-β-D-xylopyranoside	[M-H] ⁻	677.39064	677.3888	-2.7	677.3906[C ₃₇ H ₅₇ O ₁₁] ⁻ , 617.3695[C ₃₅ H ₅₃ O ₉] ⁻	46.19
56	C ₃₇ H ₅₈ O ₁₁	24-epi-24-O-acetyl-7,8-didehydrohydroshengmanol-3-O-β-D-xylopyranoside	[M-H] ⁻	677.39064	677.3888	-3.6	677.3906[C ₃₇ H ₅₇ O ₁₁] ⁻ , 635.3801[C ₃₅ H ₅₅ O ₁₀] ⁻ , 617.3695[C ₃₅ H ₅₃ O ₉] ⁻	48.05
57	C ₃₇ H ₅₆ O ₁₀	26-Deoxyactein	[M-H] ⁻	659.38007	659.3778	-3.5	659.3801[C ₃₇ H ₅₅ O ₁₀] ⁻ , 617.3695[C ₃₅ H ₅₃ O ₉] ⁻ , 599.3589 [C ₃₅ H ₅₁ O ₈] ⁻ , 559.3276[C ₃₂ H ₄₇ O ₈] ⁻ , 541.3171[C ₃₂ H ₄₅ O ₇] ⁻ , 59.0139 [C ₂ H ₃ O ₂] ⁻	49.20

58	C ₃₇ H ₅₆ O ₁₀	Cimiricaside A	[M-H] ⁻	659.38007	659.3778	-3.5	659.3801[C ₃₇ H ₅₅ O ₁₀] ⁻ ,617.3695[C ₃₅ H ₅₃ O ₉] ⁻ ,599.3589[C ₃₅ H ₅₁ O ₈] ⁻ ,581.3484[C ₃₅ H ₄₉ O ₇] ⁻ ,563.3589[C ₃₂ H ₅₁ O ₈] ⁻ ,559.3276[C ₃₂ H ₄₇ O ₈] ⁻ ,541.3535[C ₃₃ H ₄₉ O ₆] ⁻ ,59.0139[C ₂ H ₃ O ₂] ⁻	49.52
59	C ₃₇ H ₅₆ O ₁₀	CimiracemosideK	[M-H] ⁻	659.38007	659.3778	-3.5	659.3801[C ₃₇ H ₅₅ O ₁₀] ⁻ ,617.3695[C ₃₅ H ₅₃ O ₉] ⁻ ,599.3589[C ₃₅ H ₅₁ O ₈] ⁻ ,581.3484[C ₃₅ H ₄₉ O ₇] ⁻ ,559.3276[C ₃₂ H ₄₇ O ₈] ⁻ ,59.0139[C ₂ H ₃ O ₂] ⁻	49.52
60	C ₃₇ H ₅₆ O ₁₀	23-Epi-26-deoxyactein	[M-H] ⁻	659.38007	659.3778	-3.5	659.3801[C ₃₇ H ₅₅ O ₁₀] ⁻ ,617.3695[C ₃₅ H ₅₃ O ₉] ⁻ ,599.3589[C ₃₅ H ₅₁ O ₈] ⁻ ,581.3484[C ₃₅ H ₄₉ O ₇] ⁻ ,563.3589[C ₃₂ H ₅₁ O ₈] ⁻ ,541.3535[C ₃₃ H ₄₉ O ₆] ⁻ ,59.0139[C ₂ H ₃ O ₂] ⁻	49.59
61	C ₃₅ H ₅₂ O ₉	Shomaside B	[M-H] ⁻	615.35386	615.35324	-1	557.1301[C ₂₇ H ₂₅ O ₁₃] ⁻ ,471.0780[C ₁₉ H ₁₉ O ₁₄] ⁻	50.68
62	C ₃₇ H ₅₆ O ₁₀	CimiracemosideN	[M-H] ⁻	659.38007	659.3778	-4.9	659.3801[C ₃₇ H ₅₅ O ₁₀] ⁻ ,617.3695[C ₃₅ H ₅₃ O ₉] ⁻ ,599.3589[C ₃₅ H ₅₁ O ₈] ⁻ ,581.3484[C ₃₅ H ₄₉ O ₇] ⁻ ,559.3276[C ₃₂ H ₄₇ O ₈] ⁻ ,541.3171[C ₃₂ H ₄₅ O ₇] ⁻	50.75
63	C ₃₇ H ₅₆ O ₁₀	25-O-Acetyl-7,8-didehydrocimigenol 3-O-β-D-xylopyranoside	[M-H] ⁻	659.38007	659.3778	-4.9	659.3801[C ₃₇ H ₅₅ O ₁₀] ⁻ ,617.3695[C ₃₅ H ₅₃ O ₉] ⁻ ,581.3484[C ₃₅ H ₄₉ O ₇] ⁻ ,559.3276[C ₃₂ H ₄₇ O ₈] ⁻ ,541.3171[C ₃₂ H ₄₅ O ₇] ⁻	51.40
64	C ₃₅ H ₅₂ O ₈	Cimicinol	[M-H] ⁻	599.35894	599.35615	-4.7	599.3589[C ₃₅ H ₅₁ O ₈] ⁻ ,541.3171[C ₃₂ H ₄₅ O ₇] ⁻	51.45
65	C ₃₅ H ₅₂ O ₈	Cimidahuside E	[M-H] ⁻	599.35894	599.35615	-4.7	599.3589[C ₃₅ H ₅₁ O ₈] ⁻ ,541.3171[C ₃₂ H ₄₅ O ₇] ⁻	51.45
66	C ₃₉ H ₅₈ O ₁₁	2'-O-acetyl-27-deoxyactein	[M-H] ⁻	701.39064	701.38729	-4.8	701.3906[C ₃₉ H ₅₇ O ₁₁] ⁻ ,659.3801[C ₃₇ H ₅₅ O ₁₀] ⁻ ,641.3695[C ₃₇ H ₅₃ O ₉] ⁻ ,601.3382[C ₃₄ H ₄₉ O ₉] ⁻ ,583.3640[C ₃₅ H ₅₁ O ₇] ⁻ ,59.0139[C ₂ H ₃ O ₂] ⁻	52.24
67	C ₃₅ H ₅₂ O ₉	CimicifugosideH-I	[M-H] ⁻	615.35386	615.35139	-4	557.1301[C ₂₇ H ₂₅ O ₁₃] ⁻ ,471.0780[C ₁₉ H ₁₉ O ₁₄] ⁻	52.80
68	C ₃₀ H ₄₆ O ₅	24-epi-acerinol	[M-H] ⁻	485.32725	485.32486	-4.9	485.3272[C ₃₀ H ₄₅ O ₅] ⁻ ,189.1285[C ₁₃ H ₁₇ O] ⁻	53.62
69	C ₃₀ H ₄₆ O ₅	24-epi-7,8-didehydrocimigenol	[M-H] ⁻	485.32725	485.32486	-4.9	485.3272[C ₃₀ H ₄₅ O ₅] ⁻ ,189.1285[C ₁₃ H ₁₇ O] ⁻	54.03
70	C ₃₀ H ₄₆ O ₅	24-epi-Cimigenol-3-one	[M-H] ⁻	485.32725	485.32486	-4.9	485.3272[C ₃₀ H ₄₅ O ₅] ⁻ ,189.1285[C ₁₃ H ₁₇ O] ⁻	54.19
71	C ₃₀ H ₄₆ O ₅	Acerinol	[M-H] ⁻	485.32725	485.32486	-4.9	485.3272[C ₃₀ H ₄₅ O ₅] ⁻ ,189.1285[C ₁₃ H ₁₇ O] ⁻	54.19
72	C ₃₇ H ₅₄ O ₁₀	26-deoxycimicifugoside	[M-H] ⁻	657.36442	657.36147	-4.5	657.3644[C ₃₇ H ₅₃ O ₁₀] ⁻ ,597.3433[C ₃₅ H ₄₉ O ₈] ⁻	56.38
73	C ₃₇ H ₅₄ O ₁₀	Cimicifol	[M-H] ⁻	657.36442	657.36147	-4.5	657.3644[C ₃₇ H ₅₃ O ₁₀] ⁻ ,597.3433[C ₃₅ H ₄₉ O ₈] ⁻	56.38

(Continued)

Table 2 (Continued).

No.	Formula	Components	ESI	m/z Theoretical Value	m/z Actual Value	Error	Fragments	tR/ min
74	C ₃₂ H ₄₈ O ₇	12-O-Acetyllacteol	[M-H] ⁻	543.33273	543.33028	-4.5	543.3327[C ₃₂ H ₄₇ O ₇] ⁻ , 501.3222[C ₃₀ H ₄₅ O ₆] ⁻ , 483.3116[C ₃₀ H ₄₃ O ₅] ⁻ , 467.3167[C ₃₀ H ₄₃ O ₄] ⁻ , 443.2439[C ₂₆ H ₃₅ O ₆] ⁻ , 353.1970[C ₁₉ H ₂₉ O ₆] ⁻ , 59.0139[C ₂ H ₃ O ₂] ⁻	56.58
75	C ₃₂ H ₄₈ O ₇	Acetyllacteol	[M-H] ⁻	543.33273	543.33028	-4.5	543.3327[C ₃₂ H ₄₇ O ₇] ⁻ , 501.3222[C ₃₀ H ₄₅ O ₆] ⁻ , 483.3116[C ₃₀ H ₄₃ O ₅] ⁻ , 467.3167[C ₃₀ H ₄₃ O ₄] ⁻ , 443.2439[C ₂₆ H ₃₅ O ₆] ⁻ , 353.1970[C ₁₉ H ₂₉ O ₆] ⁻ , 59.0139[C ₂ H ₃ O ₂] ⁻	57.57
76	C ₁₈ H ₃₂ O ₂	Linoleic Acid	[M-H] ⁻	279.23295	279.23314	0.7	279.2330[C ₁₈ H ₃₁ O ₂] ⁻	62.67
77	C ₁₅ H ₃₀ O ₂	Pentadecanoic acid	[M-H] ⁻	241.2173	241.21782	2.1	241.2173[C ₁₅ H ₂₉ O ₂] ⁻ , 223.2067[C ₁₅ H ₂₇ O] ⁻	62.86
78	C ₁₆ H ₃₂ O ₂	Palmitic Acid	[M-H] ⁻	255.23295	255.23344	1.9	255.2330[C ₁₆ H ₃₁ O ₂] ⁻	64.55
79	C ₁₇ H ₃₄ O ₂	Methyl palmitate	[M-H] ⁻	269.2486	269.24863	0.1	269.2486[C ₁₇ H ₃₃ O ₂] ⁻	66.06
80	C ₁₈ H ₃₆ O ₂	Stearic acid	[M-H] ⁻	283.26425	283.26451	0.9	283.2643[C ₁₈ H ₃₅ O ₂] ⁻	67.42
81	C ₇ H ₁₁ N ₃ O	Cyclo-cimipronidine	[M+H] ⁺	154.09749	154.09737	-0.8	154.0975[C ₇ H ₁₂ N ₃ O] ⁺ , 112.0757[C ₆ H ₁₀ NO] ⁺ , 70.0651[C ₄ H ₈ N] ⁺	1.18
82	C ₉ H ₈ O ₄	Caffeic acid	[M+H] ⁺	181.04954	181.0495	-0.2	181.0495[C ₉ H ₉ O ₄] ⁺ , 165.0546[C ₉ H ₉ O ₃] ⁺ , 163.0390[C ₉ H ₇ O ₃] ⁺ , 135.0441[C ₈ H ₇ O ₂] ⁺ , 121.0648[C ₈ H ₉ O] ⁺ , 109.0284[C ₆ H ₅ O ₂] ⁺	5.99
83	C ₁₆ H ₂₀ O ₉	1-O-feruloyl-beta-D-glucose	[M+H] ⁺	357.11801	357.11826	0.7	195.0652[C ₁₀ H ₁₁ O ₄] ⁺ , 177.0546[C ₁₀ H ₉ O ₃] ⁺ , 149.0597[C ₉ H ₉ O ₂] ⁺ , 145.0285[C ₉ H ₅ O ₂] ⁺ , 117.0335[C ₈ H ₅ O] ⁺	6.10
84	C ₉ H ₁₀ O ₃	Paeonol	[M+H] ⁺	167.07027	167.07011	-0.6	167.0703[C ₉ H ₁₁ O ₃] ⁺ , 149.0597[C ₉ H ₉ O ₂] ⁺ , 121.0284[C ₇ H ₅ O ₂] ⁺ , 93.0335[C ₆ H ₅ O] ⁺	8.92
85	C ₁₇ H ₂₀ N ₄ O ₆	Vitamin b2	[M+H] ⁺	377.14556	377.14558	0.1	377.1456[C ₁₇ H ₂₁ N ₄ O ₆] ⁺ , 359.1350[C ₁₇ H ₁₉ N ₄ O ₅] ⁺ , 243.0877[C ₁₂ H ₁₁ N ₄ O ₂] ⁺ , 226.0611[C ₁₂ H ₈ N ₃ O ₂] ⁺ , 81.0699[C ₆ H ₉] ⁺	9.14
86	C ₁₀ H ₁₀ O ₃	(E)-3-(4-hydroxyphenyl)acrylic acid methyl ester	[M+H] ⁺	179.07027	179.0701	-1	161.0597[C ₁₀ H ₉ O ₂] ⁺ , 151.0390[C ₈ H ₇ O ₃] ⁺ , 133.0648[C ₉ H ₁₀] ⁺ , 109.0248[C ₅ H ₅ O ₂] ⁺ , 105.0699[C ₈ H ₉] ⁺ , 103.0542[C ₈ H ₇] ⁺ , 95.0491[C ₆ H ₇ O] ⁺	10.45
87	C ₁₉ H ₃₀ O ₇	Picrionoside A	[M+H] ⁺	371.20643	371.20636	-0.2	267.159[C ₁₅ H ₂₃ O ₄] ⁺ , 209.153[C ₁₃ H ₂₁ O ₂] ⁺ , 191.143[C ₁₃ H ₁₉ O] ⁺ , 149.132[C ₁₁ H ₁₇] ⁺ , 137.096[C ₉ H ₁₃ O ₄] ⁺ , 107.070[C ₄ H ₁₁ O ₃] ⁺	15.22
88	C ₂₀ H ₁₇ NO ₆	Bicuculline	[M+H] ⁺	368.11286	368.11281	-0.1	368.1129[C ₂₀ H ₁₈ NO ₆] ⁺ , 192.1019[C ₁₁ H ₁₄ NO ₂] ⁺ , 177.0182[C ₉ H ₅ O ₄] ⁺ , 174.0550[C ₁₀ H ₈ NO ₂] ⁺ , 149.0597[C ₉ H ₉ O ₂] ⁺ , 147.0441[C ₉ H ₇ O ₂] ⁺	15.82

89	C ₁₂ H ₁₄ O ₄	Ethyl ferulate	[M+H] ⁺	223.09649	223.09648	0	207.0652[C ₁₁ H ₁₁ O ₄] ⁺ , 191.0703[C ₁₁ H ₁₁ O ₃] ⁺ , 177.0546[C ₁₀ H ₉ O ₃] ⁺ , 135.0441[C ₈ H ₇ O ₂] ⁺ , 133.0648[C ₉ H ₉ O] ⁺ , 107.0491[C ₇ H ₇ O] ⁺ , 73.0284[C ₃ H ₅ O ₂] ⁺	16.04
90	C ₂₀ H ₁₇ NO ₆	Adlumidine	[M+H] ⁺	368.11286	368.11281	-0.1	368.1129[C ₂₀ H ₁₈ NO ₆] ⁺ , 192.1019[C ₁₁ H ₁₄ NO ₂] ⁺ , 177.0182[C ₉ H ₅ O ₄] ⁺ , 174.0550[C ₁₀ H ₈ NO ₂] ⁺ , 149.0597[C ₉ H ₉ O ₂] ⁺ , 147.0441[C ₉ H ₇ O ₂] ⁺	16.32
91	C ₁₅ H ₁₆ O ₆	Norcimifugin	[M+H] ⁺	293.10196	293.10216	0.7	293.1020[C ₁₅ H ₁₇ O ₆] ⁺ , 275.0914[C ₁₅ H ₁₅ O ₅] ⁺ , 233.0444[C ₁₂ H ₉ O ₅] ⁺ , 221.0444[C ₁₁ H ₉ O ₅] ⁺ , 205.0495[C ₁₁ H ₉ O ₄] ⁺	17.54
92	C ₁₉ H ₂₁ NO ₅	Tuberosine A	[M+H] ⁺	344.14925	344.14939	0.4	177.0546[C ₁₀ H ₉ O ₃] ⁺ , 151.0754[C ₉ H ₁₁ O ₂] ⁺ , 145.0284[C ₉ H ₅ O ₂] ⁺ , 117.0335[C ₈ H ₅ O] ⁺ , 91.0178[C ₆ H ₃ O] ⁺	19.58
93	C ₁₁ H ₁₂ O ₄	Caffeic acid dimethyl ether	[M+H] ⁺	209.08084	209.08055	-1.4	179.0703[C ₁₀ H ₁₁ O ₃] ⁺ , 177.0546[C ₁₀ H ₉ O ₃] ⁺ , 149.0597[C ₉ H ₉ O ₂] ⁺ , 105.0335[C ₇ H ₅ O] ⁺	21.23
94	C ₁₁ H ₁₄ O ₂	Methyleugenol	[M+H] ⁺	179.10666	179.1065	-0.9	179.1067[C ₁₁ H ₁₅ O ₂] ⁺ , 137.0597[C ₈ H ₉ O ₂] ⁺ , 135.0804[C ₉ H ₁₁ O] ⁺ , 119.0855[C ₉ H ₁₁] ⁺ , 113.0597[C ₆ H ₉ O ₂] ⁺ , 107.0491[C ₇ H ₇ O] ⁺ , 95.0855[C ₇ H ₁₁] ⁺ , 89.0597[C ₄ H ₉ O ₂] ⁺ , 67.0542[C ₅ H ₇] ⁺	21.93
95	C ₉ H ₁₀ O ₃	m-Acetoxyanisole	[M+H] ⁺	167.07027	167.07011	-1	167.0703[C ₉ H ₁₁ O ₃] ⁺ , 125.0597[C ₇ H ₉ O ₂] ⁺ , 121.0284[C ₇ H ₅ O ₂] ⁺ , 107.0491[C ₇ H ₇ O] ⁺ , 77.0386[C ₆ H ₅] ⁺	22.70
96	C ₃₅ H ₅₆ O ₁₀	21-hydroxycimigenol-3-O-β-D-xylopyranoside	[M+H] ⁺	637.39463	637.39406	-0.9	619.3841[C ₃₅ H ₅₅ O ₉] ⁺ , 487.3418[C ₃₀ H ₄₇ O ₅] ⁺ , 469.3312[C ₃₀ H ₄₅ O ₄] ⁺	23.38
97	C ₃₃ H ₄₈ O ₉	Cimilactone b	[M+H] ⁺	589.33711	589.33692	-0.3	589.3371[C ₃₃ H ₄₉ O ₉] ⁺ , 571.3265[C ₃₃ H ₄₇ O ₈] ⁺ , 553.3160[C ₃₃ H ₄₅ O ₇] ⁺ , 517.3160[C ₃₀ H ₄₅ O ₇] ⁺ , 427.2843[C ₂₇ H ₃₉ O ₄] ⁺ , 255.1591[C ₁₄ H ₂₃ O ₄] ⁺ , 161.0444[C ₆ H ₉ O ₅] ⁺	24.79
98	C ₃₅ H ₅₆ O ₁₀	Cimiricaside E	[M+H] ⁺	637.39463	637.39413	-0.8	619.3841[C ₃₅ H ₅₅ O ₉] ⁺ , 601.3735[C ₃₅ H ₅₃ O ₈] ⁺ , 547.3265[C ₃₁ H ₄₇ O ₈] ⁺ , 415.2843[C ₂₆ H ₃₉ O ₄] ⁺ , 405.2636[C ₂₄ H ₃₇ O ₅] ⁺ , 335.1853[C ₁₉ H ₂₇ O ₅] ⁺ , 159.1016[C ₈ H ₁₅ O ₃] ⁺	26.63
99	C ₃₅ H ₅₆ O ₁₀	12β-hydroxycimigenol-3-O-α-L-arabinopyranoside	[M+H] ⁺	637.39463	637.39413	-0.8	619.3841[C ₃₅ H ₅₅ O ₉] ⁺ , 601.3735[C ₃₅ H ₅₃ O ₈] ⁺ , 547.3629[C ₃₂ H ₅₁ O ₇] ⁺ , 469.3312[C ₃₀ H ₄₅ O ₄] ⁺ , 451.2690[C ₂₅ H ₃₉ O ₇] ⁺ , 423.2741[C ₂₄ H ₃₉ O ₆] ⁺	26.63
100	C ₃₂ H ₅₀ O ₇	Heracleifolinol	[M+H] ⁺	547.36293	547.36262	-0.6	547.3629[C ₃₂ H ₅₁ O ₇] ⁺ , 529.3524[C ₃₂ H ₄₉ O ₆] ⁺ , 397.2737[C ₂₆ H ₃₇ O ₃] ⁺ , 379.2115[C ₂₁ H ₃₁ O ₆] ⁺ , 201.1121[C ₁₀ H ₁₇ O ₄] ⁺ , 191.1430[C ₁₃ H ₁₉ O] ⁺	27.64
101	C ₃₇ H ₅₈ O ₁₀	25-O-Acetylcimigenol-3-O-α-L-arabinoside	[M+H] ⁺	663.41028	663.40969	-0.9	663.4103[C ₃₇ H ₅₉ O ₁₀] ⁺ , 645.3997[C ₃₇ H ₅₇ O ₉] ⁺ , 585.3786[C ₃₅ H ₅₃ O ₇] ⁺ , 531.3680[C ₃₂ H ₅₁ O ₆] ⁺ , 453.3363[C ₃₀ H ₄₅ O ₃] ⁺	27.82

(Continued)

Table 2 (Continued).

No.	Formula	Components	ESI	m/z Theoretical Value	m/z Actual Value	Error	Fragments	tR/ min
102	C ₃₅ H ₅₆ O ₁₀	Cimisine A	[M+H] ⁺	637.39463	637.39413	−0.8	619.3841[C ₃₅ H ₅₅ O ₉] ⁺ , 601.3735[C ₃₅ H ₅₃ O ₈] ⁺ , 583.3629 [C ₃₅ H ₅₁ O ₇] ⁺ , 451.2690[C ₂₅ H ₃₉ O ₇] ⁺ , 433.2585[C ₂₅ H ₃₇ O ₆] ⁺	28.39
103	C ₃₆ H ₅₆ O ₁₀	7,8-Didehydrocimigenol 3-β-D-galactopyranoside	[M+H] ⁺	649.39463	649.39397	−1	631.3841[C ₃₆ H ₅₅ O ₉] ⁺ , 631.3735[C ₃₆ H ₅₃ O ₈] ⁺ , 451.3207[C ₃₀ H ₄₃ O ₃] ⁺	29.40
104	C ₁₂ H ₈ O ₄	Norvisnagin	[M+H] ⁺	217.04954	217.04937	−0.8	217.0495[C ₁₂ H ₉ O ₄] ⁺ , 189.0546[C ₁₁ H ₉ O ₃] ⁺ , 177.0182[C ₉ H ₅ O ₄] ⁺ , 161.0233 [C ₉ H ₅ O ₃] ⁺ , 149.0233[C ₈ H ₅ O ₃] ⁺	31.68
105	C ₃₅ H ₅₄ O ₉	24-epi-7,8-didehydrocimigenol-3-O-β-D-xylopyranoside	[M+H] ⁺	619.38406	619.38365	−0.7	619.3841[C ₃₅ H ₅₅ O ₉] ⁺ , 583.3629[C ₃₅ H ₅₁ O ₇] ⁺ , 529.3524 [C ₃₂ H ₄₉ O ₆] ⁺ , 411.2894[C ₂₇ H ₃₉ O ₃] ⁺	33.70
106	C ₃₉ H ₅₈ O ₁₂	2'-O-acetylactein	[M+H] ⁺	719.4001	719.39963	−0.7	719.4001[C ₃₉ H ₅₉ O ₁₂] ⁺ , 701.3895[C ₃₉ H ₅₇ O ₁₁] ⁺ , 673.3946 [C ₃₈ H ₅₇ O ₁₀] ⁺ , 527.3367[C ₃₂ H ₄₇ O ₆] ⁺ , 351.1802[C ₁₉ H ₂₇ O ₆] ⁺ , 235.1176 [C ₁₀ H ₁₉ O ₆] ⁺	34.10
107	C ₃₉ H ₅₈ O ₁₂	Cimiracemoside O	[M+H] ⁺	719.4001	719.39963	−0.7	719.4001[C ₃₉ H ₅₉ O ₁₂] ⁺ , 673.3946[C ₃₈ H ₅₇ O ₁₀] ⁺ , 641.3684 [C ₃₇ H ₅₃ O ₉] ⁺ , 563.3215[C ₃₁ H ₄₇ O ₉] ⁺ , 527.3367[C ₃₂ H ₄₇ O ₆] ⁺ , 473.2898 [C ₂₈ H ₄₁ O ₆] ⁺ , 351.1802[C ₁₉ H ₂₇ O ₆] ⁺	34.10
108	C ₃₅ H ₅₄ O ₉	Cimiaceroside A	[M+H] ⁺	619.38406	619.38365	−0.7	619.3841[C ₃₅ H ₅₅ O ₉] ⁺ , 601.3735[C ₃₅ H ₅₃ O ₈] ⁺ , 583.3629[C ₃₅ H ₅₁ O ₇] ⁺ , 487.3418 [C ₃₀ H ₄₇ O ₅] ⁺ , 469.3312[C ₃₀ H ₄₅ O ₄] ⁺ , 451.3207[C ₃₀ H ₄₃ O ₃] ⁺ , 411.2377 [C ₂₂ H ₃₅ O ₇] ⁺ , 335.1853[C ₁₉ H ₂₇ O ₅] ⁺	34.11
109	C ₃₅ H ₅₄ O ₉	Cimidahuside H	[M+H] ⁺	619.38406	619.38365	−0.7	619.3841[C ₃₅ H ₅₅ O ₉] ⁺ , 601.3735[C ₃₅ H ₅₃ O ₈] ⁺ , 583.3629 [C ₃₅ H ₅₁ O ₇] ⁺ , 469.3312[C ₃₀ H ₄₅ O ₄] ⁺ , 451.3207[C ₃₀ H ₄₃ O ₃] ⁺ , 433.2585 [C ₂₅ H ₃₇ O ₆] ⁺	34.11
110	C ₃₇ H ₅₈ O ₁₀	23-O-Aceylshengmanol-3-O-β-D-xylopyranoside	[M+H] ⁺	663.41028	663.40896	−2	645.3997[C ₃₇ H ₅₇ O ₉] ⁺ , 585.3786[C ₃₅ H ₅₃ O ₇] ⁺ , 435.2741[C ₂₅ H ₃₉ O ₆] ⁺ , 399.2894 [C ₂₆ H ₃₉ O ₃] ⁺ , 381.2788[C ₂₆ H ₃₇ O ₂] ⁺ , 259.1540[C ₁₃ H ₂₃ O ₅] ⁺	39.35
111	C ₃₇ H ₅₈ O ₁₀	24-O-Acetyl-25-anhydroshengmanol-3-β-D-xylopyranoside	[M+H] ⁺	663.41028	663.40896	−2	645.3997[C ₃₇ H ₅₇ O ₉] ⁺ , 585.3786[C ₃₅ H ₅₃ O ₇] ⁺ , 435.2741[C ₂₅ H ₃₉ O ₆] ⁺	39.41
112	C ₃₈ H ₆₀ O ₁₁	Cimifoetiside VI	[M+H] ⁺	693.42084	693.42021	−0.9	675.4103[C ₃₈ H ₅₉ O ₁₀] ⁺ , 561.3422[C ₃₂ H ₄₉ O ₈] ⁺ , 435.2741 [C ₂₅ H ₃₉ O ₆] ⁺ , 399.2894[C ₂₆ H ₃₉ O ₃] ⁺ , 381.2788[C ₂₆ H ₃₇ O ₂] ⁺ , 337.2010 [C ₁₉ H ₂₉ O ₅] ⁺ , 259.1540[C ₁₃ H ₂₃ O ₅] ⁺	43.15

113	C ₃₅ H ₅₀ O ₈	Isocimipodocarpaside	[M+H] ⁺	599.35785	599.35727	−1	599.3578[C ₃₅ H ₅₁ O ₈] ⁺ ,467.3156[C ₃₀ H ₄₃ O] ⁺ ,449.3050[C ₃₀ H ₄₁ O ₃] ⁺ ,253.1798 [C ₁₅ H ₂₅ O ₃] ⁺	45.09
114	C ₃₇ H ₅₈ O ₁₀	23-O-Acetylshengmanol- 3-o-alpha-l-arabinopyranoside	[M+H] ⁺	663.41028	663.40917	−1.7	645.3997[C ₃₇ H ₅₇ O ₉] ⁺ ,585.3786[C ₃₅ H ₅₃ O ₇] ⁺ ,513.3575 [C ₃₂ H ₄₉ O ₅] ⁺ ,495.3469[C ₃₂ H ₄₇ O ₄] ⁺ ,453.3363[C ₃₀ H ₄₅ O ₃] ⁺ ,259.1540 [C ₁₃ H ₂₃ O ₅] ⁺	45.97
115	C ₃₇ H ₅₈ O ₁₀	24-O-Acetylisdahurinol-3-O-β- D-xylopyranoside	[M+H] ⁺	663.41028	663.40929	−1.5	645.3997[C ₃₇ H ₅₇ O ₉] ⁺ ,495.3469[C ₃₂ H ₄₇ O ₄] ⁺ ,453.3363 [C ₃₀ H ₄₅ O ₃] ⁺ ,435.2741[C ₂₅ H ₃₉ O ₆] ⁺ ,399.2894[C ₂₆ H ₃₉ O ₃] ⁺ ,381.2788 [C ₂₆ H ₃₇ O ₂] ⁺	46.33
116	C ₃₇ H ₅₈ O ₁₀	Cimicifoetiside a	[M+H] ⁺	663.41028	663.40929	−1.5	645.3997[C ₃₇ H ₅₇ O ₉] ⁺ ,585.3786[C ₃₅ H ₅₃ O ₇] ⁺ ,453.3363 [C ₃₀ H ₄₅ O ₃] ⁺ ,417.2999[C ₂₆ H ₄₁ O ₄] ⁺ ,381.2272[C ₂₁ H ₃₃ O ₆] ⁺ ,259.1176 [C ₁₂ H ₁₉ O ₆] ⁺	46.95
117	C ₃₂ H ₄₈ O ₆	25-O-Acetyl- 7,8-didehydrocimigenol	[M+H] ⁺	529.35237	529.35177	−1.1	529.3524[C ₃₂ H ₄₉ O ₆] ⁺ ,493.3312[C ₃₂ H ₄₅ O ₄] ⁺ ,469.3312 [C ₃₀ H ₄₅ O ₄] ⁺ ,451.3207[C ₃₀ H ₄₃ O ₃] ⁺ ,415.2843[C ₂₆ H ₃₉ O ₄] ⁺ ,397.2737 [C ₂₆ H ₃₇ O ₃] ⁺ ,327.2166[C ₁₈ H ₃₁ O ₅] ⁺	53.68
118	C ₃₂ H ₅₀ O ₆	Acetylshengmanol	[M+H] ⁺	531.36802	531.36733	−1.3	513.3575[C ₃₂ H ₄₉ O ₅] ⁺ ,495.3469[C ₃₂ H ₄₇ O ₄] ⁺ ,453.3363 [C ₃₀ H ₄₅ O ₃] ⁺ ,417.2999[C ₂₆ H ₄₁ O ₄] ⁺ ,337.2010[C ₁₉ H ₂₉ O ₅] ⁺ ,327.2319 [C ₂₂ H ₃₁ O ₂] ⁺ ,309.1697[C ₁₇ H ₂₅ O ₅] ⁺ ,125.0961[C ₈ H ₁₃ O] ⁺	54.28
119	C ₁₅ H ₂₆ O	beta-Eudesmol	[M+H] ⁺	223.20564	223.20552	−0.6	223.2056[C ₁₅ H ₂₇ O] ⁺ ,209.1900[C ₁₄ H ₂₅ O] ⁺ ,207.1743[C ₁₄ H ₂₃ O] ⁺ ,191.1794 [C ₁₄ H ₂₃] ⁺ ,181.1587[C ₁₂ H ₂₁ O] ⁺ ,165.1638[C ₁₂ H ₂₁] ⁺ ,153.1274 [C ₁₀ H ₁₇ O] ⁺ ,139.1481[C ₁₀ H ₁₉] ⁺ ,125.1325[C ₉ H ₁₇] ⁺	58.03
120	C ₂₀ H ₃₀ O	Vitamin A	[M+H] ⁺	287.23694	287.23693	0	287.2369[C ₂₀ H ₃₁ O] ⁺ ,269.2264[C ₂₀ H ₂₉] ⁺ ,243.2107[C ₁₈ H ₂₇] ⁺ ,177.1638 [C ₁₃ H ₂₁] ⁺ ,173.1325[C ₁₃ H ₁₇] ⁺ ,147.1168[C ₁₁ H ₁₅] ⁺	62.00
121	C ₁₀ H ₁₂ O ₂	Eugenol	[M+H] ⁺	165.09101	165.09084	−1	165.0910[C ₁₀ H ₁₃ O ₂] ⁺ ,137.0597[C ₈ H ₉ O ₂] ⁺ ,121.0648[C ₈ H ₉ O] ⁺ ,119.0831 [C ₉ H ₁₁] ⁺ ,107.0491[C ₇ H ₇ O] ⁺ ,95.0491[C ₆ H ₇ O] ⁺	67.15
122	C ₂₉ H ₄₈ O	Stigmasterol	[M+H] ⁺	413.37779	413.37741	−0.9	413.3778[C ₂₉ H ₄₉ O] ⁺ ,395.3672[C ₂₉ H ₄₇] ⁺ ,355.3359[C ₂₆ H ₄₃] ⁺ ,273.2213 [C ₁₉ H ₂₉ O] ⁺ ,259.2056[C ₁₈ H ₂₇ O] ⁺ ,255.2107[C ₁₉ H ₂₇] ⁺ ,219.2107 [C ₁₆ H ₂₇] ⁺ ,177.1274[C ₁₂ H ₁₇ O] ⁺	70.68

Network Pharmacology and Molecular Docking Validation

Screening for Potential Active Components of CR

Data on the chemical components of CR were collected from various domestic and international databases and organized, summarized, and screened through TCMSP and SwissADME searches. Seven chemical compounds, specifically isoferulic acid, ferulic acid, caffeic acid, cimifugin, cimigenol-3-O-B-D-xylopyranoside, N-cis- feruloyltyramine, and cimiside B, were not in accordance with the five principles of drug-like properties but clearly displayed anti-inflammatory activity,¹⁹ therefore, they were listed as potential effector components. A total of 23 potential active components were identified (Table 3).

Prediction of Potential Therapeutic Targets of CR

The targets of the potentially active components of CR were screened using SwissTarget prediction. After the removal of duplicates, 404 target genes were identified. The canonical names of the target genes of AP diseases were determined using GeneCards, DisGeNET, and OMIM databases, and 2255 related targets were obtained by merging and deduplication. Intersection analysis, conducted using a Venn diagram, revealed 147 intersections between CR active component targets and AP-related targets, as shown in Figure 2.

Table 3 Potential Active Components of CR

Serial Number	Chemical Composition	CAS
MOL000359	Sitosterol	83-46-5
MOL000414	Caffeate	331-39-5
MOL000449	Stigmasterol	83-48-7
MOL000483	(Z)-3-(4-hydroxy-3-methoxy-phenyl)-N-[2-(4-hydroxyphenyl)ethyl]acrylamide	80510-09-4
MOL001924	Paeoniflorin	23180-57-6
MOL002665	Ferulic Acid	1135-24-6
MOL005928	Isoferulic acid	537-73-5
MOL011734	Cimifugin	37921-38-3
MOL012023	7,8-Didehydrocimigenol	150972-72-8
MOL012052	Tuberosine A	219773-49-6
MOL012060	Cimigenol-3-O-B-D-xylopyranoside	27994-11-2
MOL012062	Cimigenol	3779-59-7
MOL012078	Visamminol	492-52-4
MOLA	Cimicifugic acid A	205114-65-4
MOLB	Cimicifugic acid B	205114-66-5
MOLC	Cimicifugic acid C	205114-67-6
MOLD	Cimicifugic acid D	219986-51-3
MOLE	Cimicifugic acid E	219986-67-1
MOLF	Peucenin	578-72-3
MOLG	Cimicinol	161239-02-7
MOLH	Acetylacteol	17503-62-7
MOLI	12β-hydroxycimigenol-3-O-α-L-arabinopyranoside	168287-99-8
MOLP	Norkhellol	4439-68-3

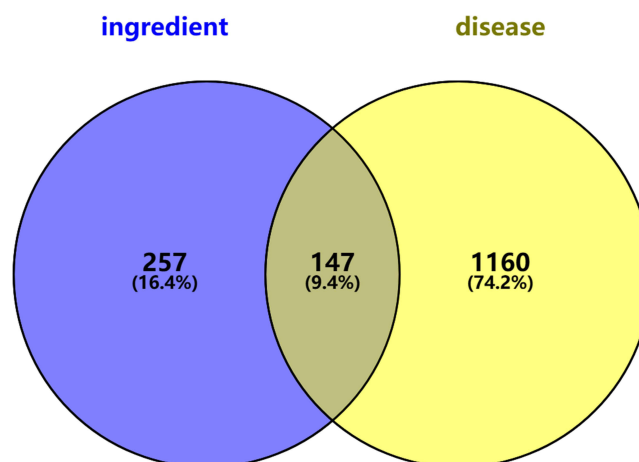


Figure 2 Venn diagram of drug-disease targets.

Construction and Analysis of the CR Active Component-Target Network

A network relationship graph of the active component targets was constructed using Cytoscape 3.10.0 software. The arrow represents the active component, the rectangle represents the potential target, and “—” represents the interaction between the active component and the target (Figure 3). Overall, 22 nodes of potential active components, 146 target nodes, and 592 edges of interactions between nodes were detected. The target network diagram of potential active components displayed the common one-to-many and many-to-one phenomena, reflecting the multi-component and multi-target characteristics of traditional Chinese medicine.

Construction and Analysis of Protein Interaction Networks (PPI)

In the protein-protein interaction network of anti-AP components of CR (Figure 4), the average degree of nodes was 12, and the screening condition for the core target set was more than twice that of the node value. The size of the node represents the degree of interaction between targets, with a higher degree corresponding to a larger node. The connecting lines between the nodes represent the interaction relationship, with higher degree values indicating closer relationships. Based on the degree, the top 15 core targets were selected (TNF, TLR4, STAT3, SRC, PIK3CA, NFKB1, JUN, JAK2, HSP90AA1, GRB2, GAPDH, EGFR, CTNNB1, BCL2, and AKT1) to construct a protein-protein interaction network diagram of core targets.

GO Functional and KEGG Enrichment Analyses of Molecules and Pathways of CR Targeting AP

The core AP targets of CR were imported into DAVID 6.8 a data platform for GO functional analysis ($P < 0.05$). As shown in Figure 5, the top 10 processes with differences in the three aspects of gene ontology (biological process, cellular composition, and molecular function) were selected for functional analysis. Biological processes mainly involve negative regulation of apoptotic processes, positive regulation of cell proliferation, positive regulation of gene expression, protein phosphorylation, response to exogenous stimuli, negative regulation of gene expression, positive regulation of protein kinase B signaling, positive regulation of protein autophosphorylation, peptidyl tyrosine phosphorylation, and positive regulation of MAP kinase activity. Cellular composition mainly involves the cytoplasm, nucleus, cytoplasm, plasma membrane, nucleoplasm, extracellular space, cell surface, macromolecular complexes, receptor complexes, and membrane rafts. Molecular functions mainly involve ATP binding, binding of identical proteins, protein serine/threonine/tyrosine kinase activity, enzyme binding, protein tyrosine kinase activity, protein kinase activity, transmembrane receptor protein tyrosine kinase activity, protein phosphatase binding, peptidase activity, and endopeptidase activity. The top 20 pathways were further selected for KEGG pathway analysis ($P < 0.05$), which revealed associations between the HIF-1 and PI3K-Akt signaling pathways and the efficacy of CR against AP (Figure 6). Chordal plots were employed to illustrate the genes enriched in the three GO processes (biological process, cellular composition, and molecular function), as well as KEGG pathways, as shown in Figure 7. The chordal plots of GO functional analysis showed that core targets

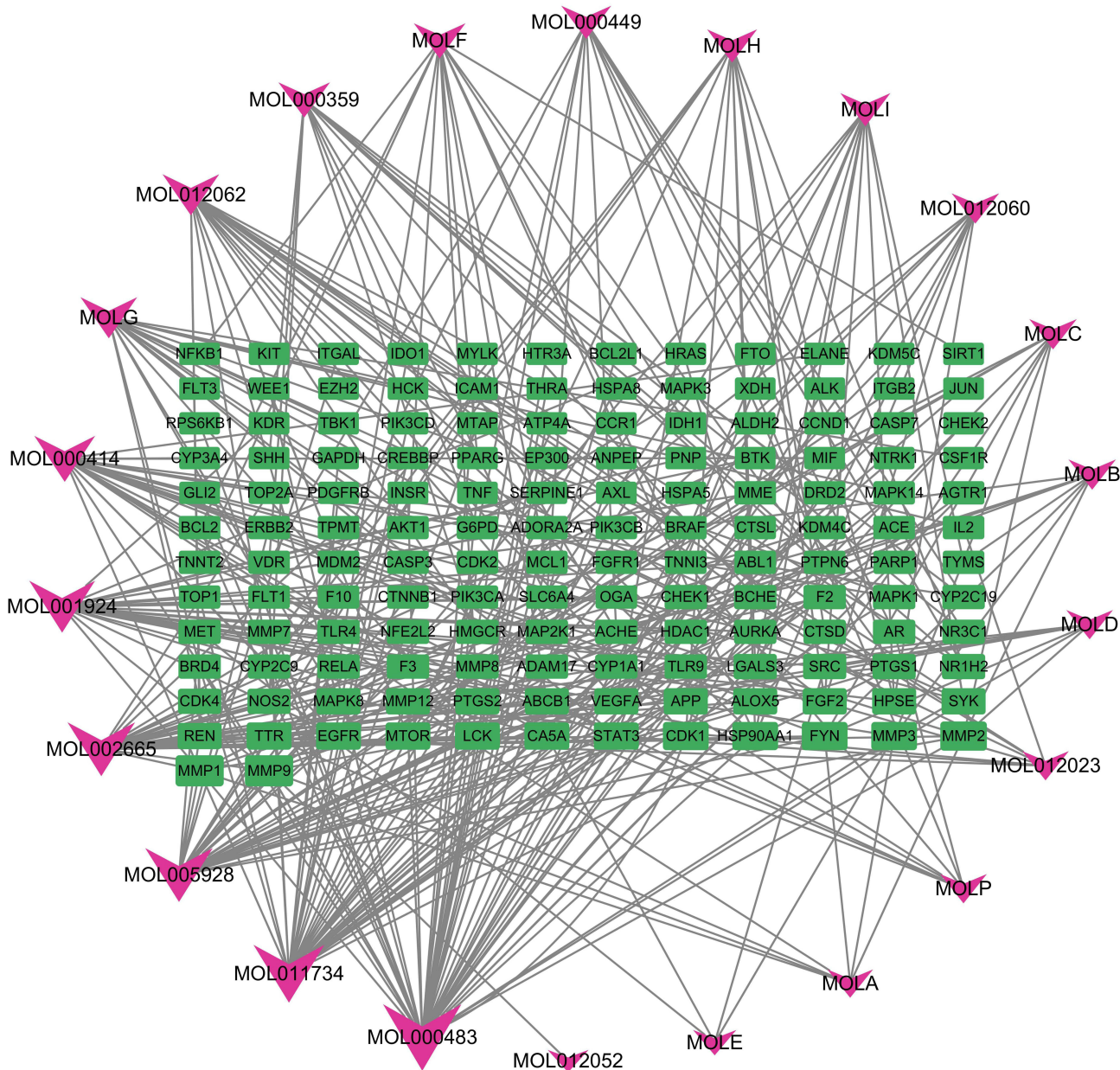


Figure 3 Active component-target network relationship diagram: 22 nodes of potential active components, 146 target nodes, and 592 edges of interactions between nodes were detected.

of CR were mainly enriched in biological processes, such as negative regulation of apoptotic process (GO: 0043066), positive regulation of cell proliferation (GO: 0008284), positive regulation of gene expression (GO: 0010628), response to exogenous stimuli (GO: 0009410), and protein phosphorylation (GO: 0006468), and primarily involved cytoplasm (GO: 0005737), cytoplasmic lysosomes (GO: 0005829), nuclei (GO: 0005634), plasma membrane (GO: 0005886), and nucleoplasm (GO: 0005654), among other cellular components. The key targets were mainly involved in the following molecular functions: protein serine/threonine/tyrosine kinase activity (GO:0004712), enzyme binding (GO:0019899), ATP binding (GO:0005524), identical protein binding (GO:0042802), and protein kinase activity (GO:0004672). The core protein targets were TNF-, TLR4, STAT3, SRC, PIK3CA, NFKB1, JUN, JAK2, HSP90AA1, GRB2, GAPDH, EGFR, CTNNB1, BCL2, and AKT1. KEGG chordal maps showed that TLR4, HSP90AA1, and PIK3CA were significantly implicated in the regulation of HIF-1 (hsa04066) and the PI3K-Akt signaling pathway (hsa04151), which involved STAT3, GAPDH, TLR4, and PIK3CA as primary targets. Notably, a single target was involved in the regulation

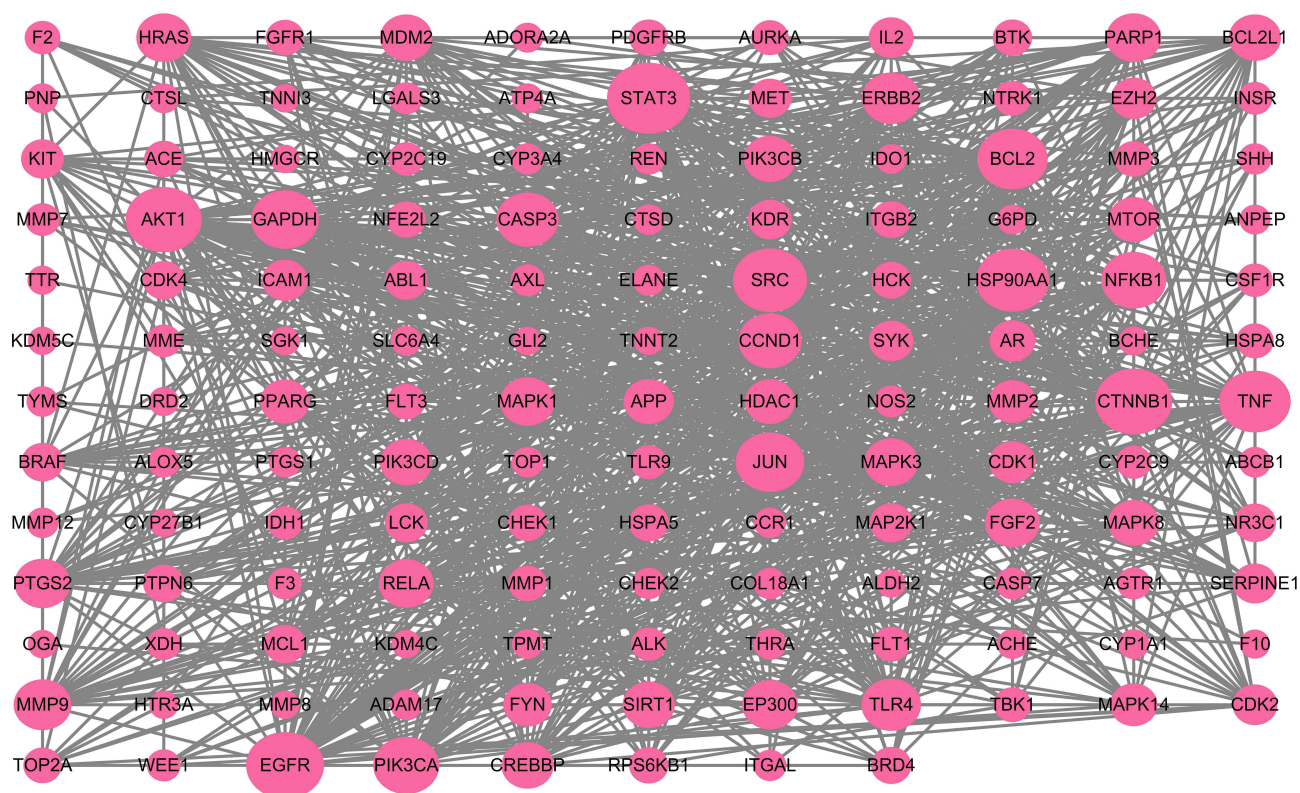


Figure 4 Network diagram of protein interactions: the average degree of nodes was 12.

of both the HIF-1 signaling pathway (hsa04066) and PIK3CA (hsa04151). Thus, a target could be simultaneously involved in different pathways, and a single pathway could be enriched for multiple targets. Two core targets, PIK3CA and TLR4, are involved in most of the pathways.

Molecular Docking of Potential Active Components to Core Targets

According to the active component-target network diagram, the top 10 potential active components were selected based on their degree values (outlined in Table 4). Most of the active compounds identified were phenolic acids, highlighting the possibility that the effectors exerting therapeutic effects on AP are phenolic acid components. The 10 selected components were molecularly docked with 15 core protein targets using the AutoDock software, and 150 docking binding energies were obtained (Figure 8). The parameters of molecular ID and chemical structure of the docked proteins are listed in Table 4. Among these, CR displayed the lowest binding energies to GAPDH and JAK2, followed by TNF-, EGFR, and TLR4. Lower docking binding energies indicate that CR binds to these targets with higher affinity, indicating a higher likelihood of action on these specific targets, which would influence their structure and function and, consequently, the regulation of the corresponding signaling pathways.

Docking data were analyzed using heat maps (Figure 8). The depth of the color represents the absolute value of the binding energy, with a deeper color corresponding to a larger absolute value and stronger binding effect. The results revealed a docking binding energy of <0 kJ/mol, indicating that the selected components effectively bound to their protein targets. The top four components ranked by degree were MOL000483, MOL011734, MOL005928, and MOL0026654, which represented N-cis-feruloyltyramine, ferulic acid, cimifugin, and isoferulic acid, respectively.

Using PyMOL software, small molecules with top-degree rankings that could represent potentially active components with strong protein interactions were visualized (Figure 9). MOL000483 formed hydrogen bonds with the amino acid residues ASN-287, SER-51, THR-52, ALA-238, and GLN-204 in GAPDH (Figure 9A) and GLY-239 in PIK3CA (Figure 9B). MOL005928 formed hydrogen bonds with residues ASP-93, SER52, and LYS-58 on HSP90AA1 (Figure 9C) and LEU-564 and GLN-436 on TLR4 (Figure 9D). MOL011734 formed hydrogen bonds with residues

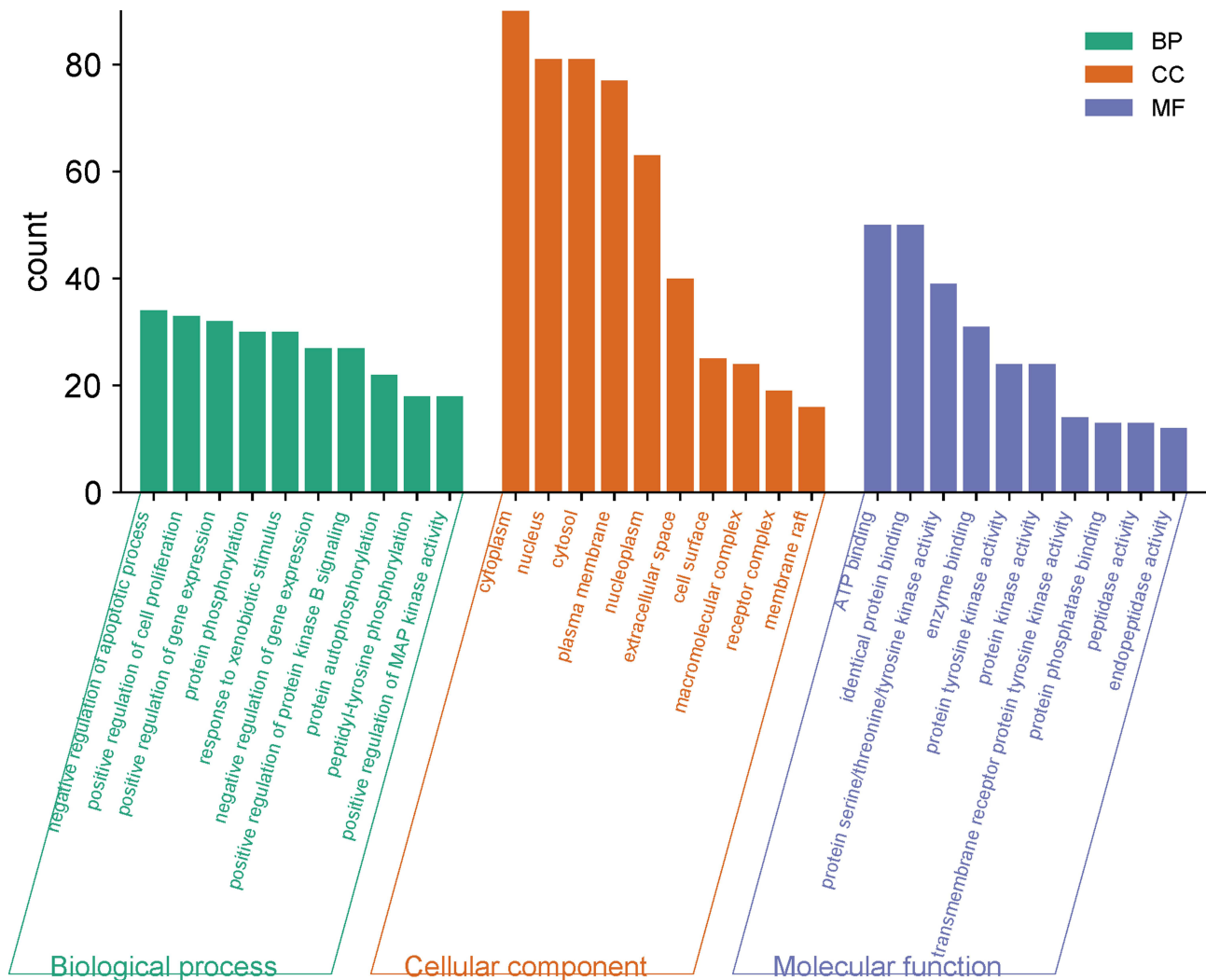


Figure 5 GO enrichment analysis: the top 10 processes with differences in the three aspects of gene ontology (biological process, cellular composition, and molecular function) were selected for functional analysis.

ASN-287 and ALA-238 in GAPDH (Figure 9E) as well as TYR-26 in PIK3CA (Figure 9F). MOL002665 formed hydrogen bonds with residues ALA-238, ASN-239, and LEU-203 in GAPDH (Figure 9G) as well as LYS-58 in HSP90AA1 (Figure 9H).

Based on the collective data, four main components of CR, specifically N-cis- feruloyltyramine, ferulic acid, cimifugin, and isoferulic acid, have been proposed to exert therapeutic effects against AP by modulating several proteins, including GAPDH, PIK3CA, TLR4, and HSP90AA1, as well as their related signaling pathways. Additional in vitro cellular experiments were conducted to validate these components and target proteins.

In vitro Experimental Validation

Effect of Different LPS Concentrations on BEAS-2B Cell Proliferation

The results of CCK-8 experiments showed that LPS had a significant inhibitory effect on the proliferation of BEAS-2B cells at a certain concentration compared with the control group ($P < 0.05$). At concentrations below 75 $\mu\text{g/mL}$, no significant differences were observed between the control and experimental groups ($P > 0.05$), indicating that LPS did not exert a notable toxic effect on cells within this concentration range. Consequently, this concentration range was identified as a safe range for drug administration, and the corresponding experimental results are presented in Figure 10.

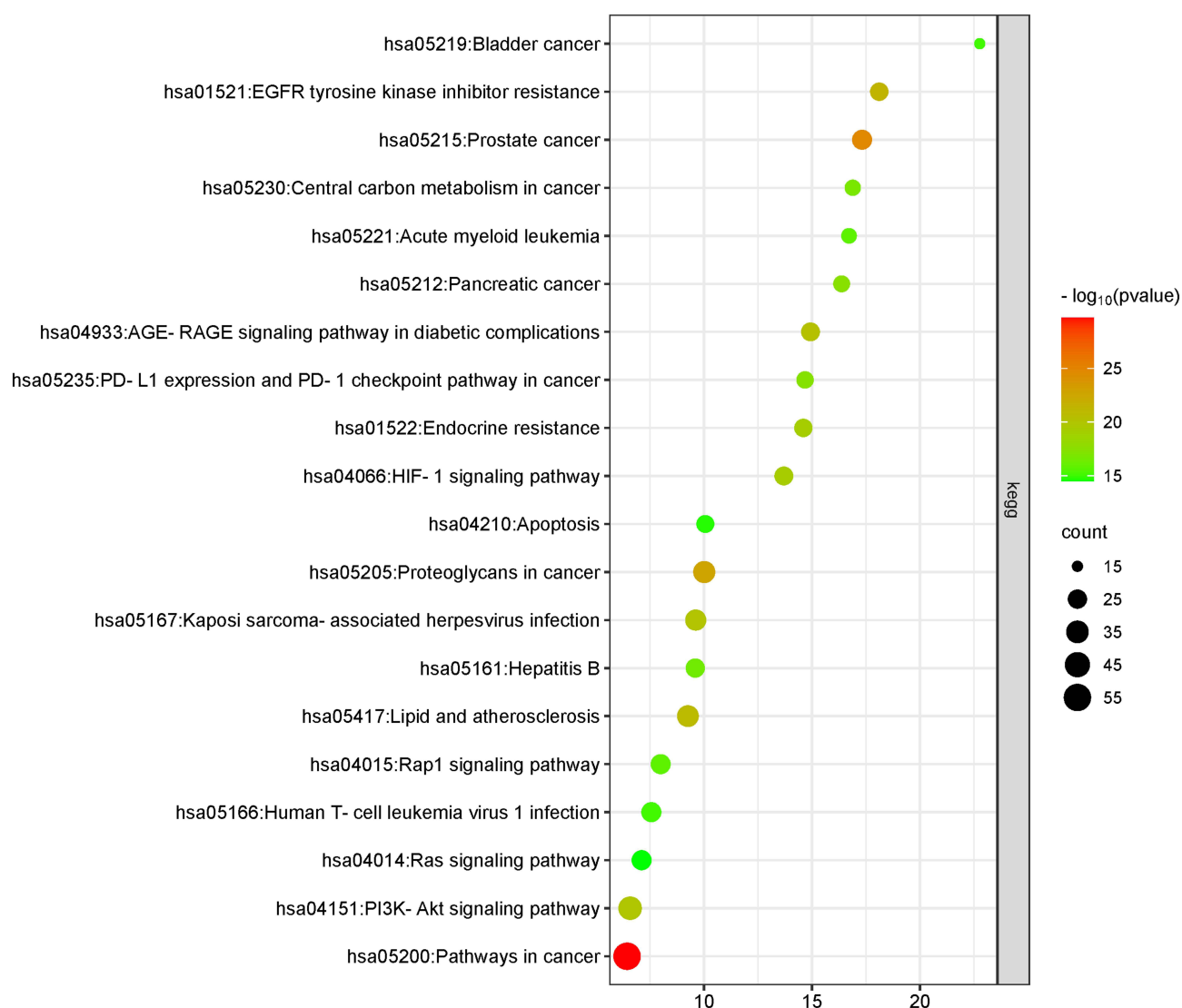


Figure 6 The top 20 pathways were selected for KEGG pathway analysis ($P < 0.05$).

Effects of CR Effector Components on Expression of Inflammatory Factors

The results of the ELISA experiments (Figure 11) showed that compared with the control group, the expression levels of the inflammatory factors TNF- α , IL-1 β , and IL-6 were significantly increased in the model group. Notably, the expression levels of TNF- α , IL-1 β , and IL-6 decreased to different degrees in the groups treated with cimifugin, isoferulic acid, ferulic acid, and N-cis- feruloyltyramine, relative to the model group. Our findings indicated that the potentially active components of CR exert different degrees of inhibitory effects on inflammatory factors.

Effects of CR Effector Components on TLR4, PIK3CA, and HSP90AA1 mRNA Expression

RT-qPCR data (Figure 12) showed that compared with the control group, the mRNA expression of *TLR4* and *PIK3CA* in the model group was significantly increased, while that of *HSP90AA1* was significantly decreased. Notably, compared with the model group, cells treated with cimifugin, isoferulic acid, ferulic acid, and N-cis- feruloyltyramine showed downregulation of *TLR4* and *PIK3CA* and significant upregulation of *HSP90AA1* mRNA.

Effects of CR Effector Components on TLR4, PIK3CA, HSP90AA1, STAT3 and p-STAT3 Proteins

Western blot analysis (Figure 13) showed that the protein expression of TLR4 and PIK3CA was significantly increased, whereas that of HSP90AA1 was significantly decreased in the model group compared with that in the control group.

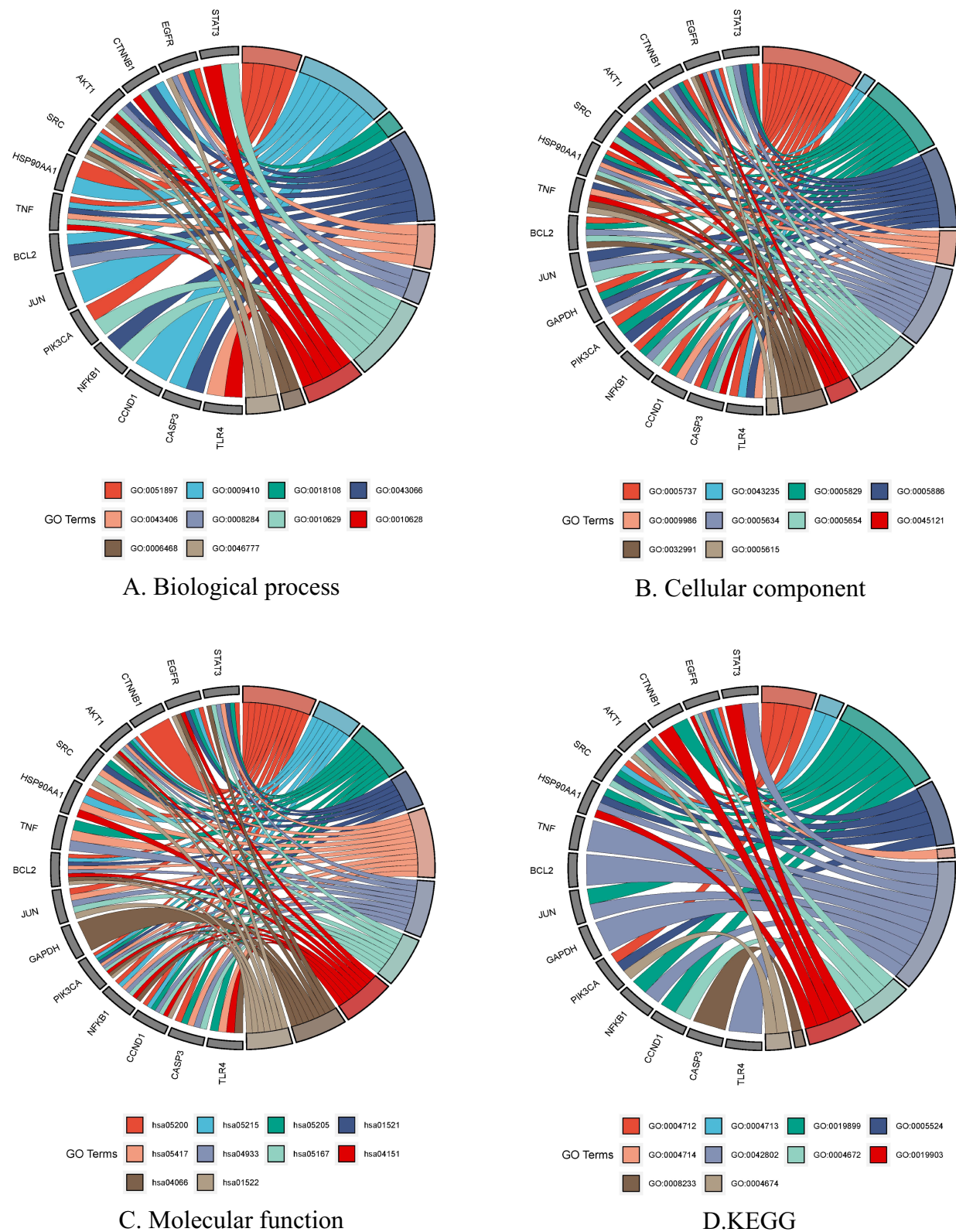
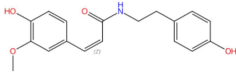
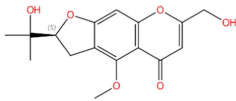
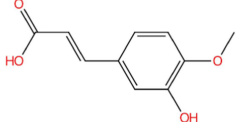
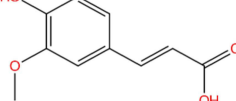
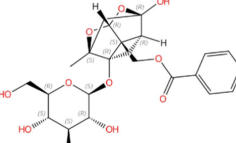
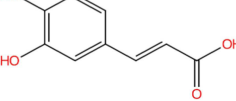
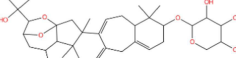

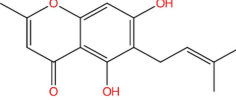


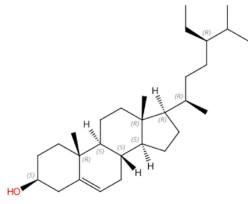
Figure 7 String diagrams of GO and KEGG: (A) Biological process, (B) Cellular component, (C) Molecular function, (D) KEGG.

Table 4 Structures of the Potential Active Components Used for Molecular Docking

Serial Number No.	Molecule ID	Chemical Structure
No. 1	MOL000483	
No. 2	MOL011734	
No. 3	MOL005928	
No. 4	MOL002665	
No. 5	MOL001924	
No. 6	MOL000414	
No. 7	MOLG	
No. 8	MOL012062	
No. 9	MOLF	

(Continued)

Table 4 (Continued).

Serial Number No.	Molecule ID	Chemical Structure
No. 10	MOL000359	

Relative to the model group, the expression levels of TLR4 and PIK3CA in the cimifugin, isoferulic, ferulic, and N-cis-feruloyltyramine treatment groups decreased to varying degrees, whereas that of the HSP90AA1 protein was markedly increased. No significant differences in STAT3 protein expression levels were observed among the control, model, and drug treatment groups ($P>0.05$). The expression of the p-STAT3 protein in the cells of the model group was significantly higher than that in the control group. Notably, in the cimifugin, isoferulic acid, ferulic acid, and N-cis-feruloyltyramine groups, p-STAT3 protein expression in cells was significantly reduced relative to that in the model group.

Discussion

According to data from the 2019 Global Burden of Disease (GBD) study, lower respiratory tract infections (LRTIs), including pneumonia and bronchiolitis, are the leading causes of mortality from infectious diseases worldwide, accounting for more deaths than tuberculosis or AIDS. AP can be caused by a combination of multiple microorganisms (bacteria, viruses, chlamydia, mycoplasma, or rickettsia) or individual infections, primarily manifesting clinically as fever, cough, or dyspnea. Based on these clinical symptoms, AP is classified as a phlegm-heat congestion of lung syndrome in Chinese

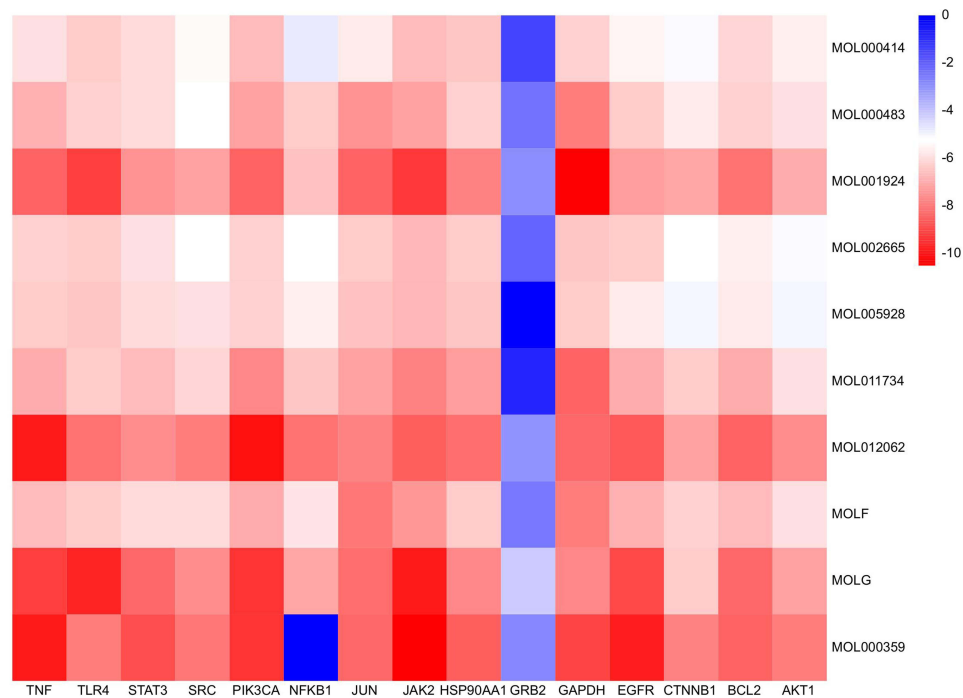


Figure 8 Heat map analysis of the molecular docking results.

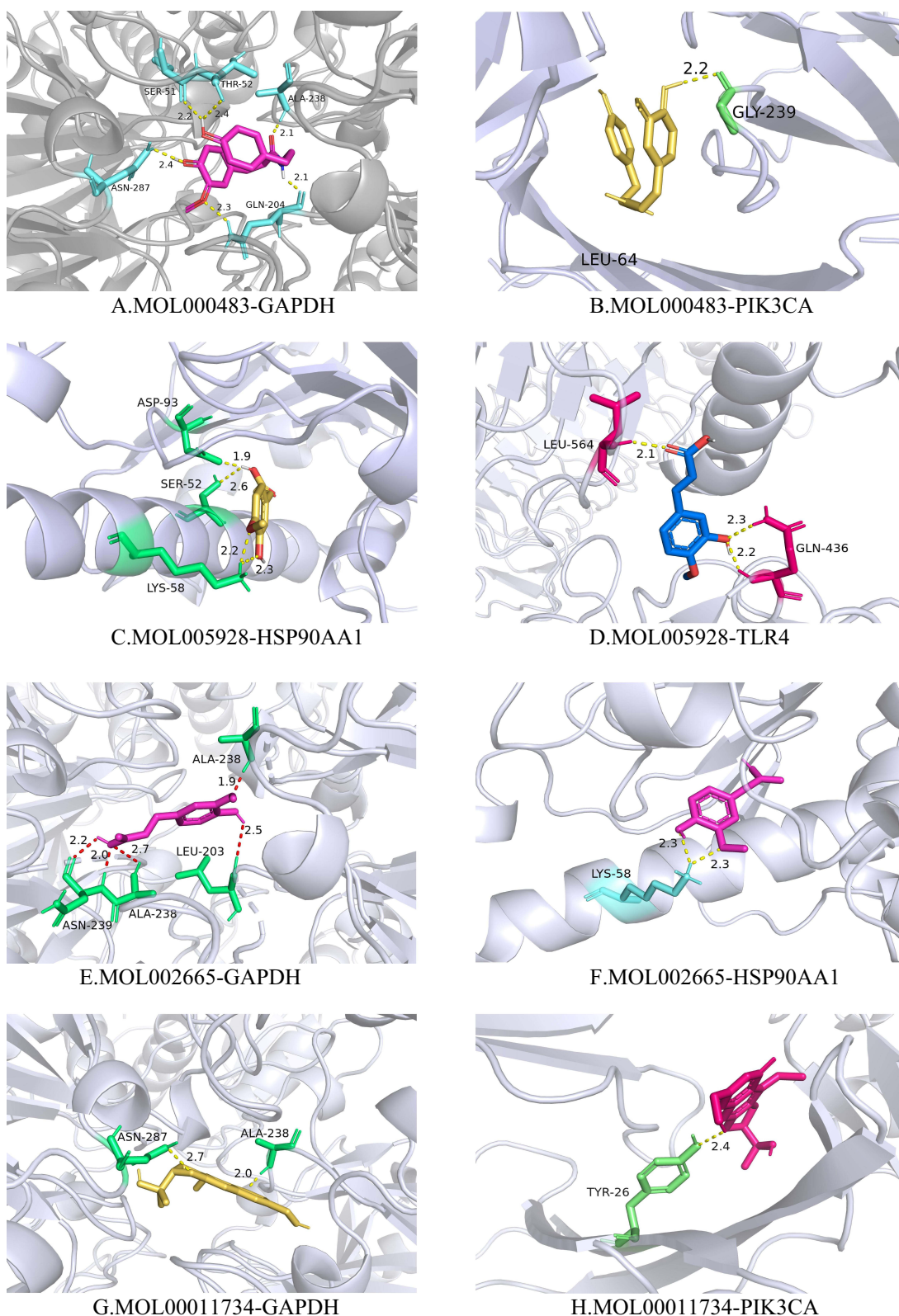


Figure 9 Molecular docking diagrams of potential active components of CR with protein targets: **(A)** Visualization of predicted binding mode of MOL000483 (N-cis-feruloyltyramine) and GAPDH, **(B)** Visualization of predicted binding mode of MOL000483 (N-cis-feruloyltyramine) and PIK3CA, **(C)** Visualization of predicted binding mode of MOL005928 (Isoferulic acid) and HSP90AA1, **(D)** Visualization of predicted binding mode of MOL005928 (Isoferulic acid) and TLR4, **(E)** Visualization of predicted binding mode of MOL002665 (Ferulic Acid) and GAPDH, **(F)** Visualization of predicted binding mode of MOL002665 (Ferulic Acid) and HSP90AA1, **(G)** Visualization of predicted binding mode of MOL00011734 (Cimifugin) and GAPDH, **(H)** Visualization of predicted binding mode of MOL00011734 (Cimifugin) and PIK3CA.

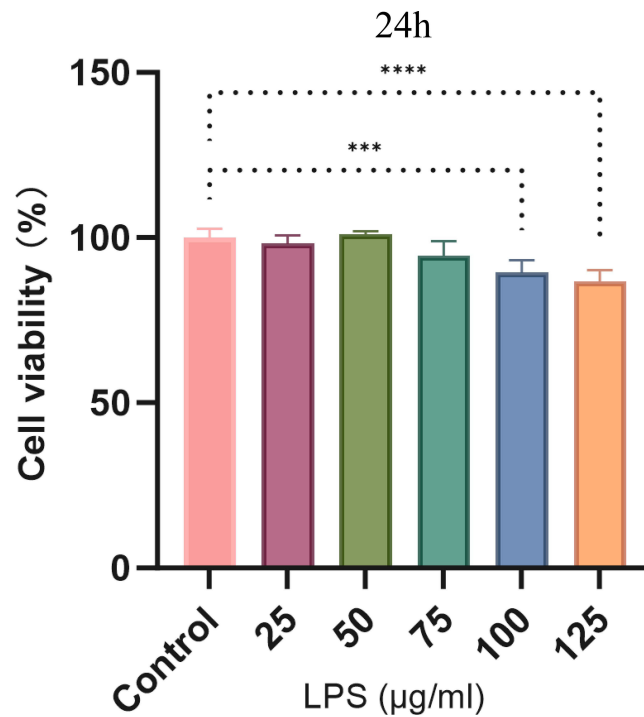


Figure 10 CCK-8 assay to determine cell viability of BEAS-2B cells after LPS stimulation for 24 h. (**p < 0.001, ***p < 0.001 vs control group).

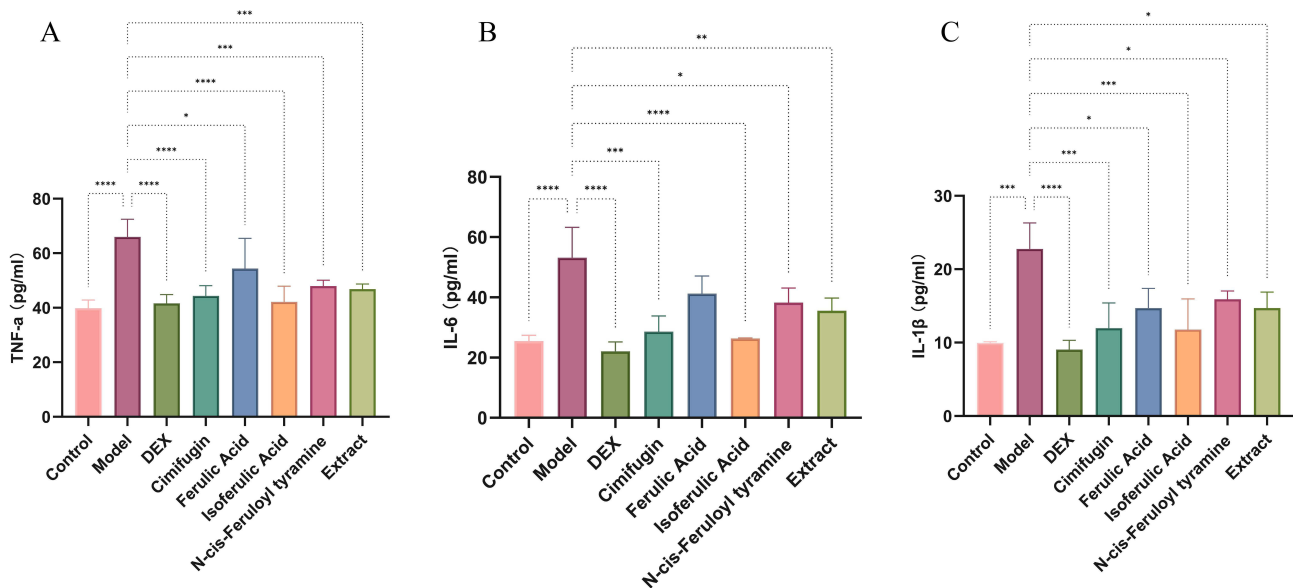


Figure 11 ELISA kits were used to measure levels of (A) TNF-α, (B) IL-6, and (C) IL-1β. (*p < 0.05, **p < 0.01, ***p < 0.001, ****p < 0.001 vs model group).

medicine.²⁰ Heat and toxicity stagnation in the lungs have been reported to cause lung carbuncles.²¹ The ability of CR to clear heat and detoxify toxins has also been previously reported. In particular, the phenolic acid component of CR has strong anti-inflammatory and antiviral pharmacological activities, and can be effectively used to treat epiganglionic heat-toxicity syndrome of gingivitis, mouth and tongue sores, sore throat, and pestilence toxins. CR extracts inhibit the expression of inflammatory factors, exert a protective effect against lung injury induced by *Pseudomonas aeruginosa* infection,²² and suppress allergic asthma in rats by modulating the Nrf 2/HO-1/NQO 1 signaling pathway.¹⁹ Previous

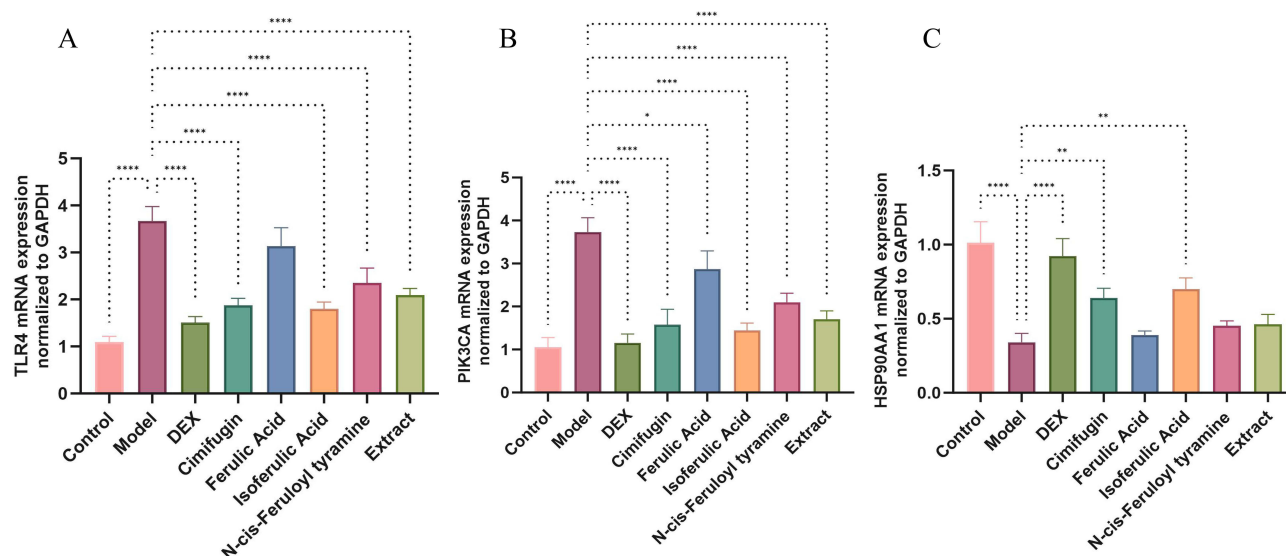


Figure 12 RT-qPCR was used to detect the expression of (A) TLR4, (B) PIK3CA and (C) HSP90AA1. (* $p < 0.05$, ** $p < 0.01$, *** $p < 0.001$ vs model group).

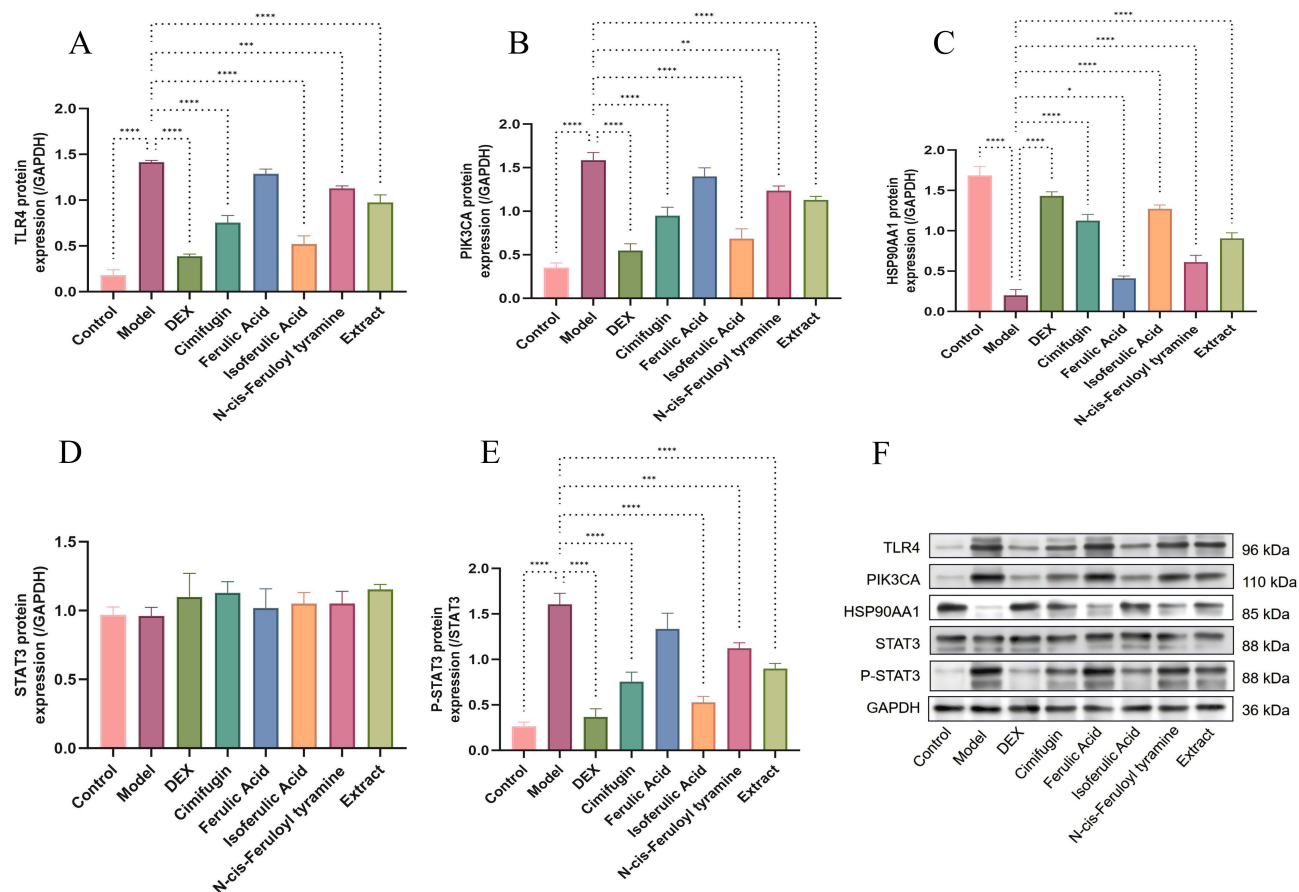


Figure 13 WB was used to detect the expression of (A) TLR4/GAPDH, (B) PIK3CA/GAPDH, (C) HSP90AA1/GAPDH, (D) STAT3/GAPDH, (E) p-STAT3/STAT3, and (F) Western Blot. (* $p < 0.05$, ** $p < 0.01$, *** $p < 0.001$, **** $p < 0.0001$ vs model group).

studies have demonstrated that ferulic acid and isoferulic acid in CR prevent the infiltration of neutrophils into the lungs of influenza mice,^{22,23} clearly supporting their therapeutic effect on lung diseases.

In this study, network pharmacology was employed, involving the construction of a “component-target” network, along with molecular docking simulation and validation experiments, which revealed N-cis- feruloyltyramine,^{24,25} ferulic acid, isoferulic acid,^{26,27} and cimifugin^{28–30} are likely to be the active effector components of CR against acute pneumonia. For these components screened out by Network Pharmacology but not identified by us, we also measured the levels of CR using HPLC to ensure that the components we screened out were actually present in CR. Studies have shown that these compounds suppress the expression of inflammatory factors, NO, PGE2, and other inflammation-related indicators, and exert anti-inflammatory and protective effects on lung tissues through modulation of signaling pathways, such as NF- κ B, MAPK, or JAK/STAT3, with utility in the treatment of inflammation-related diseases in the lung. The data from in vitro cellular experiments are consistent with the above findings. Phenolic acids (N-cis- feruloyltyramine, ferulic acid, and isoferulic acid) and chromones (cimifugin) in CR inhibit inflammatory factor expression and exert therapeutic effects. Accordingly, we performed in vitro cellular experiments to verify whether the four components of CR are effector components with anti-AP activity, and human normal lung epithelial cells (BEAS-2B) are commonly used to explore AP, lung injury, and other diseases.^{31–33} Lipopolysaccharide (LPS), a major membrane component of gram-negative bacteria, is extremely toxic to respiratory cells and a potent inducer of pro-inflammatory activity, effectively mimicking bacterial stimulation of cells to produce inflammatory responses.^{34–36} In the current study, the BEAS-2B cell line was selected for experiments, and LPS was used to induce significant upregulation of IL-6, TNF- α , IL-1 β , and other factors to mimic inflammation in lung epithelial cells. Data from network pharmacology analysis suggest that CR and its effector components exert therapeutic effects in acute pneumonia by modulating the PI3K-Akt and JAK/STAT3 signaling pathways. PIK3CA, TLR4, STAT3, and P-STAT3 were identified as indicators of pathways involved in molecular docking and binding in subsequent in vitro cellular experiments. Three inflammatory factors, TNF- α , IL-1 β , and IL-6, were significantly expressed in the LPS model group, indicating that LPS stimulated BEAS-2B cells to produce an inflammatory response. The expression levels of these inflammatory factors significantly decreased after treatment, suggesting that both CR alcoholic extracts and individual effector components have anti-inflammatory activities, and consequently, therapeutic effects. This validates the predictions of network pharmacology.

The mRNA and protein levels of TLR4 and PIK3CA in the model group were significantly increased, whereas TLR4 and PIK3CA protein expression was significantly decreased after administration of CR, suggesting that anti-inflammatory and anti-injury effects are potentially exerted through the downregulation of TLR4 and PIK3CA and subsequent inhibition of the PI3K-Akt signaling pathway. Accordingly, CR alcohol extract and its effector components have been proposed to exert therapeutic effects against AP by downregulating inflammatory factors, hindering the occurrence of cytokine storms, and inhibiting excessive immune activation. Western blot analysis revealed no significant differences in STAT3 expression between groups. However, the expression of p-STAT3 in the cells of the model group was markedly elevated compared to that in the control group, clearly indicating that LPS induces the phosphorylation of STAT3 in cells. Based on these results, we propose that LPS promotes the expression of the phosphorylated STAT3 protein, which is significantly inhibited by CR and its active components. HSP90AA1 is a molecular chaperone that binds to bacterial lipopolysaccharide (LPS) and mediates the LPS-induced inflammatory response. HSP90AA1 expression was significantly reduced in the model group and increased after the administration of the drug or its active components. One potential explanation for this finding is that the effector component blocks LPS-induced inflammatory response by preventing the binding of HSP90AA1. IL-1 β , IL-6, TNF- α ,^{34–36} and other specific cytokines overactivate JAK/STAT3 signaling, leading to sequential activation and phosphorylation of JAKs and STAT3. Phosphorylated STAT3 forms homodimers and translocates to the nucleus, where it binds to the promoter regions of target genes and activates transcription, which, in turn, regulates the expression of other inflammatory factors and induces more severe inflammatory responses. Cis-N-feruloyltyrosine amine, ferulic acid, cimifugin, and isoferulic acid modulate the IL-6/JAK/STAT3 signaling pathway by inhibiting the expression of IL-1 β , IL-6, and TNF- α cytokines and blocking the phosphorylation of STAT3. TLR4 is a major lipopolysaccharide (LPS) receptor belonging to the Toll receptor family³⁶ and its activation by LPS stimulates MyD88 and trimeric (IL-1 β and IL-1RI bound to IL-1RAcP) interactions,^{37,38} inducing phosphorylation of IRAK. Subsequently, phosphorylated IRAK promotes the oligomerization of tumor necrosis factor-related factor 6 (TRAF6), which triggers the activation of the NF- κ B³⁹ and

MAPK signaling pathways,⁴⁰ stimulating the expression of inflammatory factors. N-cis- feruloyltyramine, cimifugin, and isoferulic acid potentially regulate TLR4/IL-1 β -IRAK/NF- κ B signaling by inhibiting the expression of IL-1 β and TLR4. *PIK3CA* which belongs to the PI3K-Akt signaling pathway, encodes p110 α protein. Elevated expression of this gene increases the risk of mutation. Substitution of *PIK3CA* triggers a state of continuous mutation and activation of PI3K enzymes. Moreover, changes in *PIK3CA* induce other downstream PI3K kinases and enhance intracellular signaling, which in turn stimulates the activation of the entire pathway and produces a pro-inflammatory effect that exacerbates the development of inflammatory diseases.⁴¹ N-cis- feruloyltyramine, cimifugin, and isoferulic acid appeared to regulate the PI3K-Akt signaling pathway by inhibiting the expression of *PIK3CA* protein. In conclusion, N-cis- feruloyltyramine, ferulic acid, cimifugin, and isoferulic acid function collaboratively through a range of signaling pathways as the active components of CR to exert therapeutic effects on AP.

Conclusion

In the current study, N-cis- feruloyltyramine, ferulic acid, cimifugin, and isoferulic acid in CR were identified as the effector components of AP activity through network pharmacology in combination with cellular experiments. Our collective data indicate that these components co-regulate IL-6/JAK/STAT3 signaling by inhibiting cytokines, such as IL-6, TNF- α , and IL-1 β , as well as downregulating P-STAT3, TLR4, and *PIK3CA*, which are involved in the TLR4/IL-1 β -IRAK/NF- κ B and PI3K-Akt signaling pathways.

Data Sharing Statement

The datasets used and/or analyzed during the current study are available from the corresponding author upon reasonable request.

Acknowledgments

The authors are thankful to the Jiangxi University of Chinese Medicine for their assistance in conducting this study.

Author Contributions

All authors made a significant contribution to the work reported, whether that is in the conception, study design, execution, acquisition of data, analysis and interpretation, or in all these areas; took part in drafting, revising or critically reviewing the article; gave final approval of the version to be published; have agreed on the journal to which the article has been submitted; and agree to be accountable for all aspects of the work.

Funding

This work was supported by National Key Research and Development Program (2023YFC3504204); The Jiangxi Province ‘Double Thousand Talents’ High-end Talent Program for Youth in Science and Technology Innovation (No. xsg2023201117), Jiangxi Provincial Academic and Technical Leaders of Major Disciplines Young Talents Training Program (No. 20212BCJ23019), Jiangxi Provincial Natural Science Foundation (No. 20224BAB216102), Jiangxi University of Chinese Medicine Traditional Chinese Medicine Concoctions Technology Inheritance Innovation Team Construction Project (No. CXTD22003).

Disclosure

The authors declare that the research was conducted in the absence of any commercial or financial relationships that could be construed as a potential conflict of interest.

References

- Long ME, Mallampalli RK, Horowitz JC. Pathogenesis of pneumonia and acute lung injury. *Clin Sci*. 2022;136(10):747–769. doi:10.1042/CS20210879
- Gu D, Dong N, Zheng Z, et al. A fatal outbreak of ST11 carbapenem-resistant hypervirulent *Klebsiella pneumoniae* in a Chinese hospital: a molecular epidemiological study. *Lancet Infect Dis*. 2018;18(1):37–46. doi:10.1016/S1473-3099(17)30489-9

3. Wang Z, Cai R, Wang G, et al. Combination Therapy of Phage vB_KpnM_P-KP2 and Gentamicin Combats Acute Pneumonia Caused by K47 Serotype *Klebsiella pneumoniae*. *Front Microbiol.* **2021**;12:674068.
4. Chen R, Luo YP, Xu XH, Miao Q, Wang YG. Traditional Chinese Medicine Diagnosis and Treatment of 52 Cases of Coronavirus Disease 2019 (COVID-19) in Wuhan and Analysis of Typical Medical Cases. *J Tradit Chin Med.* **2020**;61(09):741–744.
5. Li PF, Liu CX. Origin, Changes and Analysis of Efficacy of Cimicifugae Rhizoma. *Chin J Exp Traditional Med Formulae.* **2022**;28(7):218–226.
6. Zhu J, Yuan E, Chen XL, Chen Q, Zhong LY, Ye XD. Effect of Jiangxi Characteristic Processing Technology on Volatile Components of Cimicifugae Rhizoma. *Chin J Exp Traditional Med Formulae.* **2019**;25(21):95–105.
7. Ji ZL, Zhou H, Wang JF, Han LY, Zheng CJ, Chen YZ. Traditional Chinese medicine information database. *J Ethnopharmacol.* **2006**;103(3):501. doi:10.1016/j.jep.2005.11.003
8. Ru J, Li P, Wang J, et al. TCMSP: a database of systems pharmacology for drug discovery from herbal medicines. *J Cheminf.* **2014**;6(1):13. doi:10.1186/1758-2946-6-13
9. Lipinski CA, Lombardo F, Dominy BW, Feeney PJ. Experimental and computational approaches to estimate solubility and permeability in drug discovery and development settings. *Adv Drug Delivery Rev.* **2012**;64:4–17. doi:10.1016/j.addr.2012.09.019
10. Zhang W, Xue K, Gao Y, et al. Systems pharmacology dissection of action mechanisms of Dipsaci Radix for osteoporosis. *Life Sci.* **2019**;235:116820. doi:10.1016/j.lfs.2019.116820
11. Stelzer G, Rosen N, Plaschkes I, et al. The GeneCards Suite: from Gene Data Mining to Disease Genome Sequence Analyses. *Curr protoc bioinf.* **2016**;54(1):1.30.1–1.30.33. doi:10.1002/cpbi.5
12. Yu Y, Zhang G, Han T, Huang H. Analysis of the pharmacological mechanism of Banxia Xiexin decoction in treating depression and ulcerative colitis based on a biological network module. *BMC Complement Med Therap.* **2020**;20(1):199. doi:10.1186/s12906-020-02988-3
13. Zhu N, Hou J. Exploring the mechanism of action Xianlingubao Prescription in the treatment of osteoporosis by network pharmacology. *Comput Biol Chem.* **2020**;85:107240. doi:10.1016/j.compbiolchem.2020.107240
14. Li WH, Han JR, Ren PP, Xie Y, Jiang DY. Exploration of the mechanism of Zisheng Shenqi decoction against gout arthritis using network pharmacology. *Comput Biol Chem.* **2021**;90:107358. doi:10.1016/j.compbiolchem.2020.107358
15. Cui Q, Liang ZY, hui MY, et al. A network pharmacology approach to investigate the mechanism of Shuxuening injection in the treatment of ischemic stroke. *J Ethnopharmacol.* **2020**;257:112891. doi:10.1016/j.jep.2020.112891
16. Zhang J, Huang Q, Zhao R, Ma Z. A network pharmacology study on the Tripterygium wilfordii Hook for treatment of Crohn's disease. *BMC Complement Med Therap.* **2020**;20(1):95. doi:10.1186/s12906-020-02885-9
17. Gegen ZL, Gao Y, Site GL, Alatan CLM, Tai BLH, Tu Y. Mechanism of Syringa oblata in treating angina pectoris based on GC-MS and network pharmacology. *China J Chinese Materia Medica.* **2022**;47(3):836–845. doi:10.19540/j.cnki.cjcmm.20210927.201
18. Liu Z, Liu R, Wang R, et al. Sinenetin attenuates IL-1 β -induced cartilage damage and ameliorates osteoarthritis by regulating SERPINA3. *Food Funct.* **2022**;13(19):9973–9987. doi:10.1039/D2FO01304E
19. Yang X, Liu Y, Gan J, Xiao ZX, Cao Y. FitDock: protein–ligand docking by template fitting. *Briefings Bioinf.* **2022**;23(3):bbac087. doi:10.1093/bib/bbac087
20. Lim JO, Song KH, Lee IS, et al. Cimicifugae Rhizoma Extract Attenuates Oxidative Stress and Airway Inflammation via the Upregulation of Nrf2/HO-1/NQO1 and Downregulation of NF- κ B Phosphorylation in Ovalbumin-Induced Asthma. *Antioxidants.* **2021**;10(10):1626. doi:10.3390/antiox10101626
21. Xiong XD, Zhou JY, Cao KY, Yan HP, Zhao M. Clinical Observation on 60 Patients with Acute Pneumonia (Type of Phlegm-Heat Obstructing Lungs) Treated by Tanreqing Injecion. *J Emergency Traditional Chin Med.* **2003**;12(2):97–98.
22. Hu YL. An Analysis of heat toxin. *World Latest Medicine Information.* **2016**;16(90):258–261.
23. Hu L, Song X, Nagai T, et al. Chemical profile of Cimicifuga heracleifolia Kom. And immunomodulatory effect of its representative bioavailable component, cimigenoside on Poly(I:C)-induced airway inflammation. *J Ethnopharmacol.* **2021**;267:113615. doi:10.1016/j.jep.2020.113615
24. Hirabayashi T, Ochiai H, Sakai S, Nakajima K, Terasawa K. Inhibitory Effect of Ferulic Acid and Isoferulic Acid on Murine Interleukin-8 Production in Response to Influenza Virus Infections in vitro and in vivo. *Planta Med.* **1995**;61(03):221–226. doi:10.1055/s-2006-958060
25. Hwang JT, Kim Y, Jang HJ, et al. Study of the UV Light Conversion of Feruloyl Amides from Portulaca oleracea and Their Inhibitory Effect on IL-6-Induced STAT3 Activation. *Molecules.* **2016**;21(7):865. doi:10.3390/molecules21070865
26. Lu Q, Zhang WY, Pan DB, et al. Phenolic acids and their glycosides from the rhizomes of Cimicifuga dahurica. *Fitoterapia.* **2019**;134:485–492. doi:10.1016/j.fitote.2019.03.023
27. Sakai S, Kawamata H, Kogure T, et al. Inhibitory Effect of Ferulic Acid and Isoferulic Acid on the Production of Macrophage Inflammatory Protein-2 in Response to Respiratory Syncytial Virus Infection in RAW264.7 Cells. *Mediators Inflamm.* **1999**;8(3):346214. doi:10.1080/09629359990513
28. Wang ZY, Wang Q, Han YQ, et al. Bioactivity-based UPLC/Q-TOF/MS strategy for screening of anti-inflammatory components from Cimicifugae Rhizoma. *Chin Chem Lett.* **2017**;28(2):476–481. doi:10.1016/j.cclet.2016.11.021
29. Liu A, Zhao W, Zhang B, Tu Y, Wang Q, Li J. Cimifugin ameliorates imiquimod-induced psoriasis by inhibiting oxidative stress and inflammation via NF- κ B/MAPK pathway. *Biosci Rep.* **2020**;40(6):BSR20200471. doi:10.1042/BSR20200471
30. Chen JJ, Yang DW. Inhibitory effect of cimifugin on allergic inflammation in bronchial epithelial cells via NF- κ B pathway. *Chin J Immunol.* **2024**;40(3):534–539.
31. Jiang Q, Yi M, Guo Q, et al. Protective effects of polydatin on lipopolysaccharide-induced acute lung injury through TLR4-MyD88-NF- κ B pathway. *Int Immunopharmacol.* **2015**;29(2):370–376. doi:10.1016/j.intimp.2015.10.027
32. Han Y, Ge C, Ye J, Li R, Zhang Y. Demethyleneberberine alleviates *Pseudomonas aeruginosa*-induced acute pneumonia by inhibiting the AIM2 inflammasome and oxidative stress. *Pulmonary Pharmacol Therapeut.* **2023**;83:102259. doi:10.1016/j.pupt.2023.102259
33. Lei Y, Zhu Y, Mallah MA, et al. The activation of SIRT1 ameliorates BPDE-induced inflammatory damage in BEAS-2B cells via HMGB1/TLR4/NF- κ B pathway. *Environ Toxicol.* **2023**;38(10):2429–2439. doi:10.1002/tox.23878
34. Reutershan J, Basit A, Galkina EV, Ley K. Sequential recruitment of neutrophils into lung and bronchoalveolar lavage fluid in LPS-induced acute lung injury. *Am J Physiol Lung Cell Mol Physiol.* **2005**;289(5):L807–L815. doi:10.1152/ajplung.00477.2004
35. Lu Y, Wu Y, Huang M, et al. Fuzhengjiedu formula exerts protective effect against LPS-induced acute lung injury via gut-lung axis. *Phytomedicine.* **2024**;123:155190. doi:10.1016/j.phymed.2023.155190

36. Zeng Z, Fu Y, Li M, Shi Y, Ding Q, Chen S. Guben Qingfei decoction attenuates LPS-induced acute lung injury by modulating the TLR4/NF- κ B and Keap1/Nrf2 signaling pathways. *J Ethnopharmacol.* **2024**;323:117674. doi:10.1016/j.jep.2023.117674
37. Ciesielska A, Matyjek M, Kwiatkowska K. TLR4 and CD14 trafficking and its influence on LPS-induced pro-inflammatory signaling. *Cell Mol Life Sci.* **2021**;78(4):1233–1261.
38. Netea MG, van Deven de Veerdonk FL, van der Meer JWM, Dinarello CA, Joosten LAB. Inflammasome-Independent Regulation of IL-1-Family Cytokines. *Ann Rev Immunol.* **2015**;33(2015):49–77. doi:10.1146/annurev-immunol-032414-112306
39. Kwak A, Lee Y, Kim H, Kim S. Intracellular interleukin (IL)-1 family cytokine processing enzyme. *Arch Pharm Res.* **2016**;39(11):1556–1564. doi:10.1007/s12272-016-0855-0
40. Moynagh PN. The NF- κ B pathway. *J Cell Sci.* **2005**;118(20):4589–4592. doi:10.1242/jcs.02579
41. Rocha DM, Caldas AP, Oliveira LL, Bressan J, Hermsdorff HH. Saturated fatty acids trigger TLR4-mediated inflammatory response. *Atherosclerosis.* **2016**;244:211–215. doi:10.1016/j.atherosclerosis.2015.11.015
42. Chen K, Iribarren P, Gong W, Wang JM. The Essential Role of Phosphoinositide 3-Kinases (PI3Ks) in Regulating Pro-Inflammatory Responses and the Progression of Cancer. *Cell Mol Immunol.* **2005**;2(4):241–252.

Journal of Inflammation Research

Publish your work in this journal

The Journal of Inflammation Research is an international, peer-reviewed open-access journal that welcomes laboratory and clinical findings on the molecular basis, cell biology and pharmacology of inflammation including original research, reviews, symposium reports, hypothesis formation and commentaries on: acute/chronic inflammation; mediators of inflammation; cellular processes; molecular mechanisms; pharmacology and novel anti-inflammatory drugs; clinical conditions involving inflammation. The manuscript management system is completely online and includes a very quick and fair peer-review system. Visit <http://www.dovepress.com/testimonials.php> to read real quotes from published authors.

Submit your manuscript here: <https://www.dovepress.com/journal-of-inflammation-research-journal>

Dovepress
Taylor & Francis Group